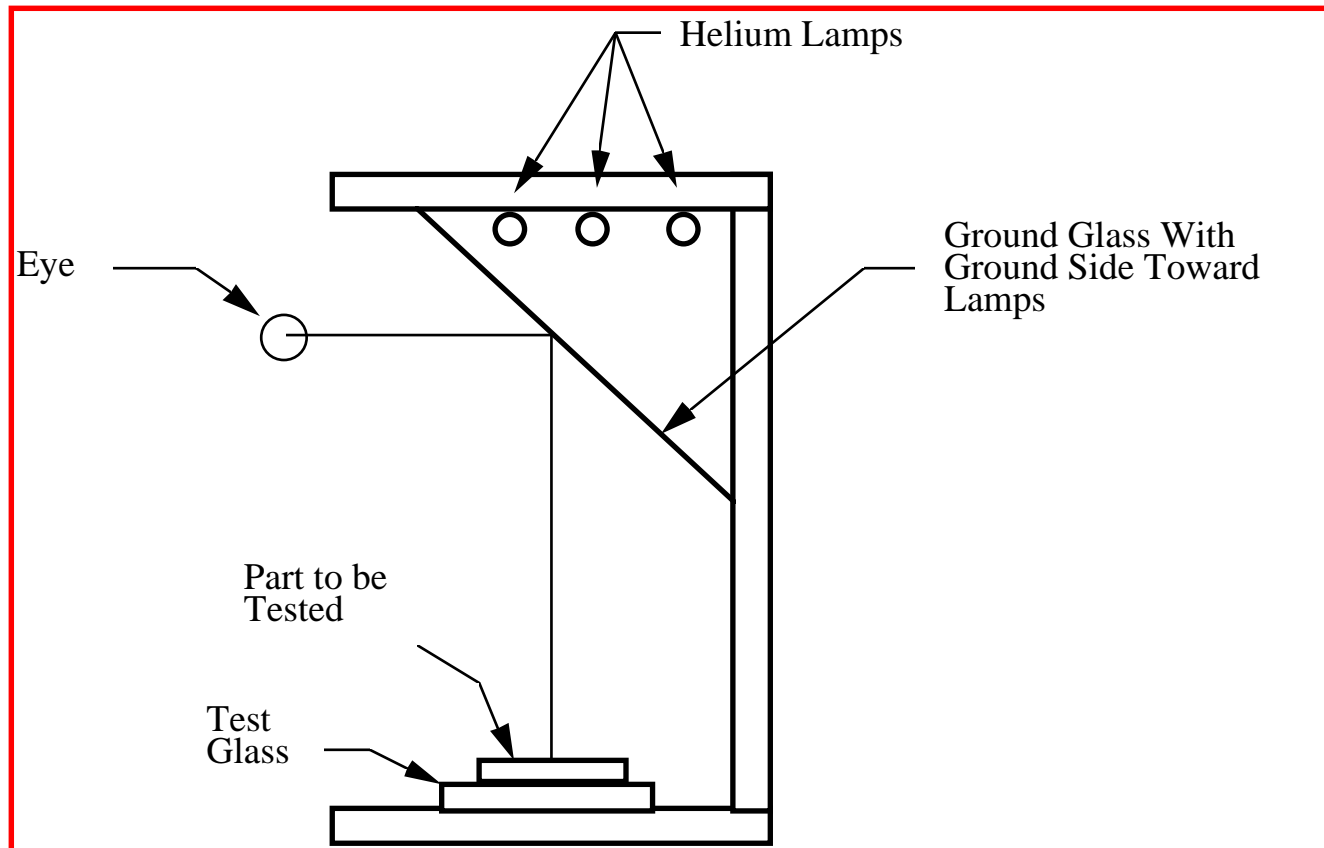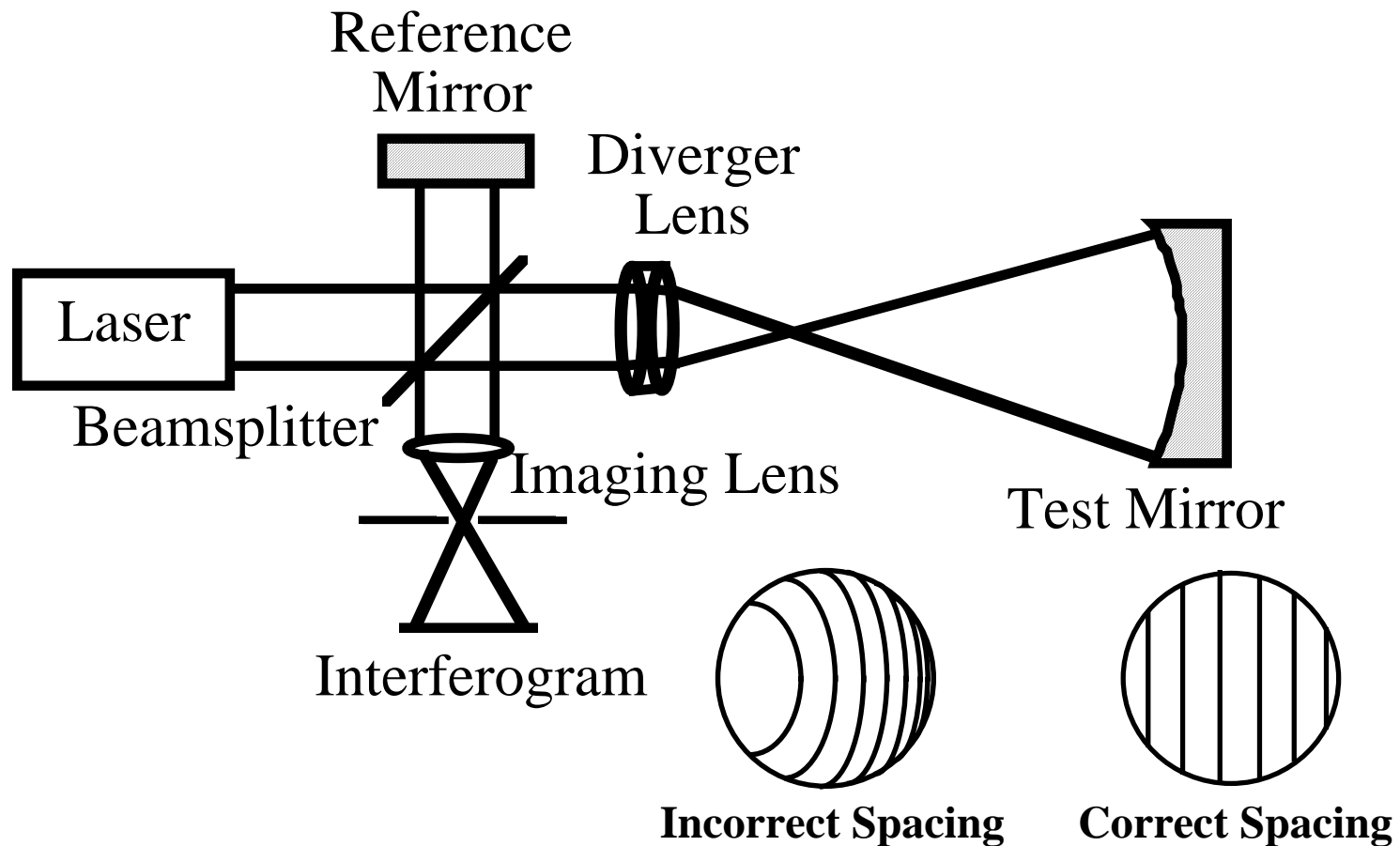Testing Curved Surfaces and Lenses
1. Test Plate
2. Twyman-Green Interferometer (LUPI)
3. Fizeau (Laser source)
4. Shack Cube Interferometer
5. Scatterplate Interferometer
6. Smartt Point Diffraction Interferometer
7. Sommargren Diffraction Interferometer
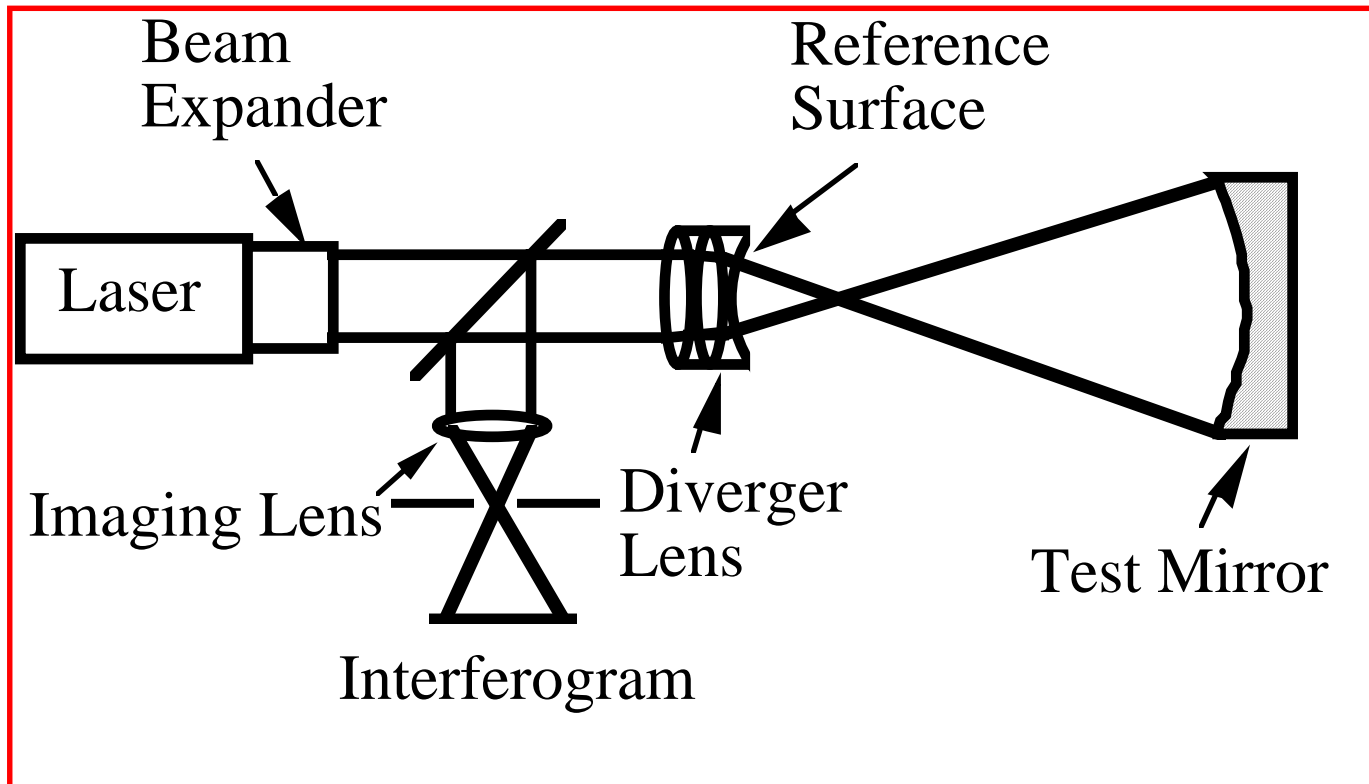8. Measurement of Cylindrical Surfaces
9. Star Test
10. Shack-Hartmann Test

Classical Fizeau Interferometer

Helium Lamps

Ground Glass With Ground Side Toward Lamps

Eye

Part to be Tested

Test Glass

Twyman-Green Interferometer (Spherical Surfaces)

Reference Mirror

Diverger Lens

Laser

Beamsplitter

Imaging Lens

Test Mirror

Interferogram

Incorrect Spacing

Correct Spacing

Fizeau Interferometer-Laser Source (Spherical Surfaces)

Beam Expander

Reference Surface

Laser

Imaging Lens

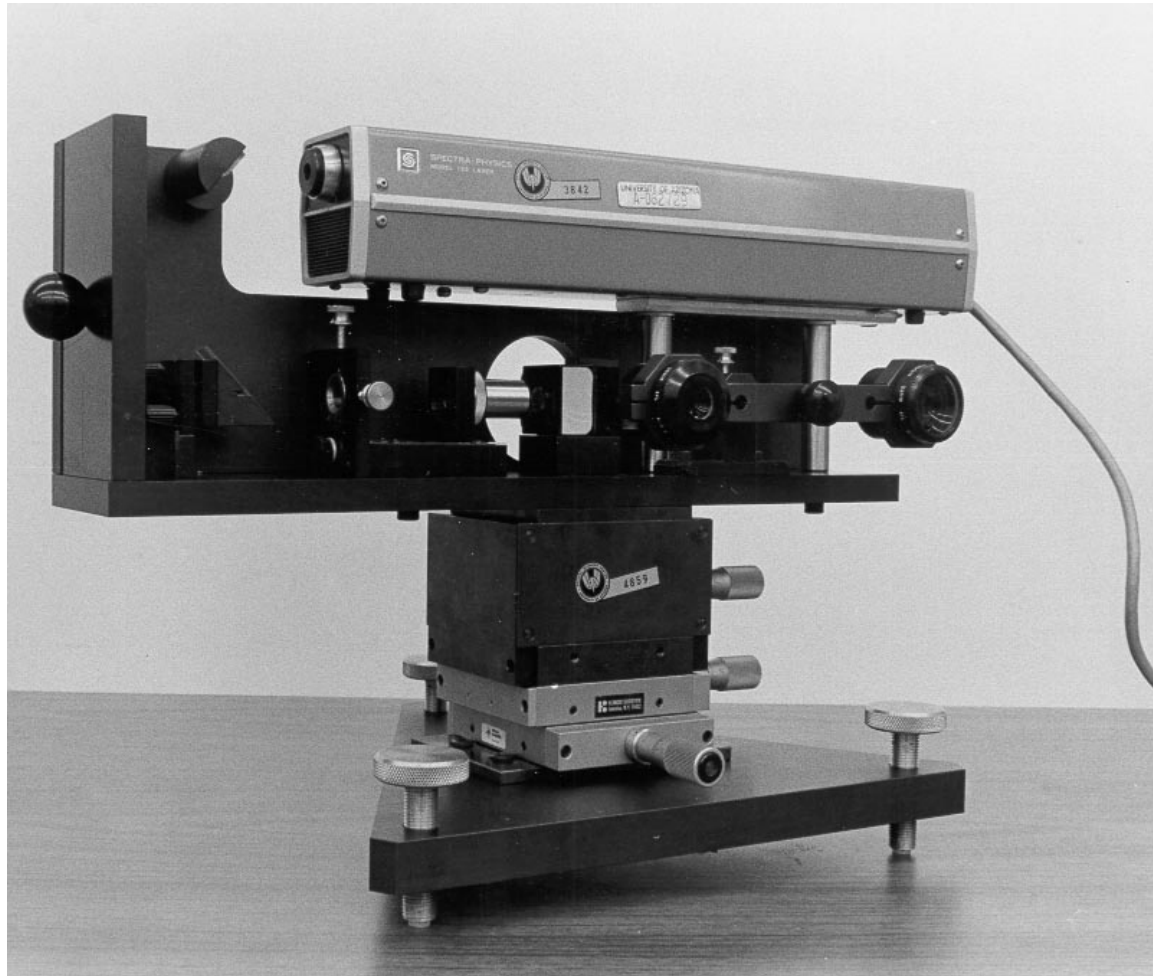Diverger Lens

Interferogram

Test Mirror

Shack Interferometer
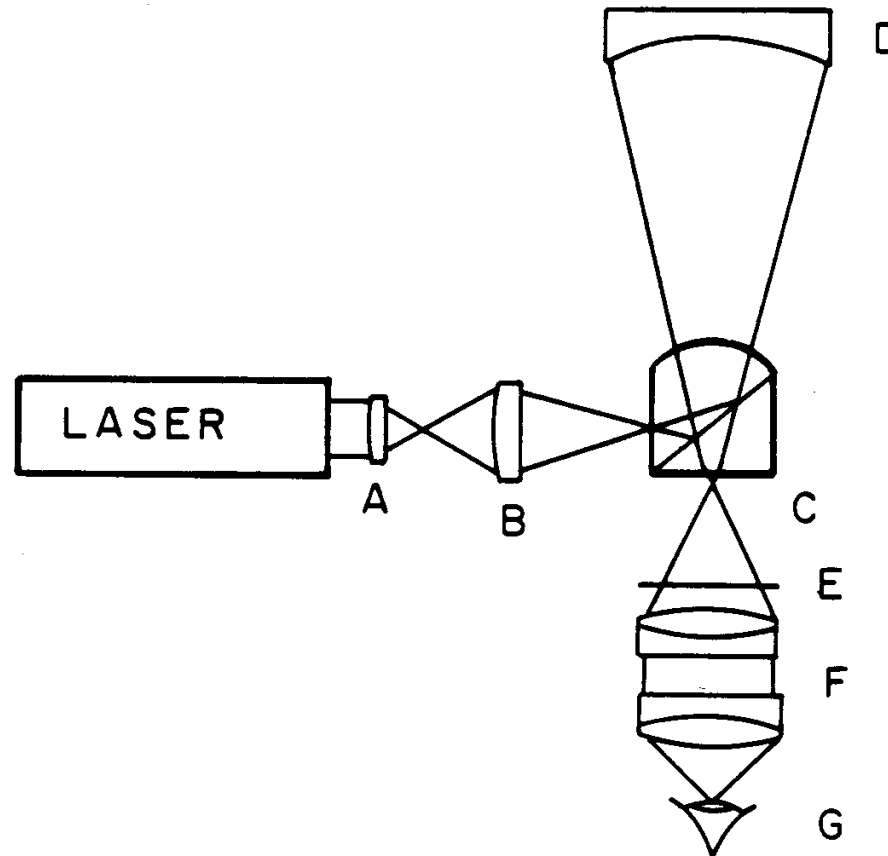
Ref: R. V. Shack and G. W. Hopkins, Opt. Eng. 18, p. 226, March-April 1979

Shack Interferometer

1998 - James C. Wyant

8.2.6 Scatterplate Interferometer

The scatterplate interferometer illustrated in Fig. 8.2.6-1 for the testing of a spherical mirror gives fringes of constant contour just as does the LUPI; however, its operation does not depend on the knowledge of the quality of auxiliary optics. Due to the common path feature of the interferometer, the light source can be either a laser, or more commonly, a white light source such as a zirconium arc or tungsten bulb with a Wratten spectral filter. The light source is focused onto a pinhole, which is then reimaged onto the surface under test. A scatterplate a few millimeters in diameter is placed at the center of curvature of the mirror under test. Part of the light illuminating the scatterplate will pass unscattered to focus directly on the mirror surface, while part of the light will be scattered uniformly over the mirror surface. The mirror will reimage the scatterplate back on itself--inverted, of course.
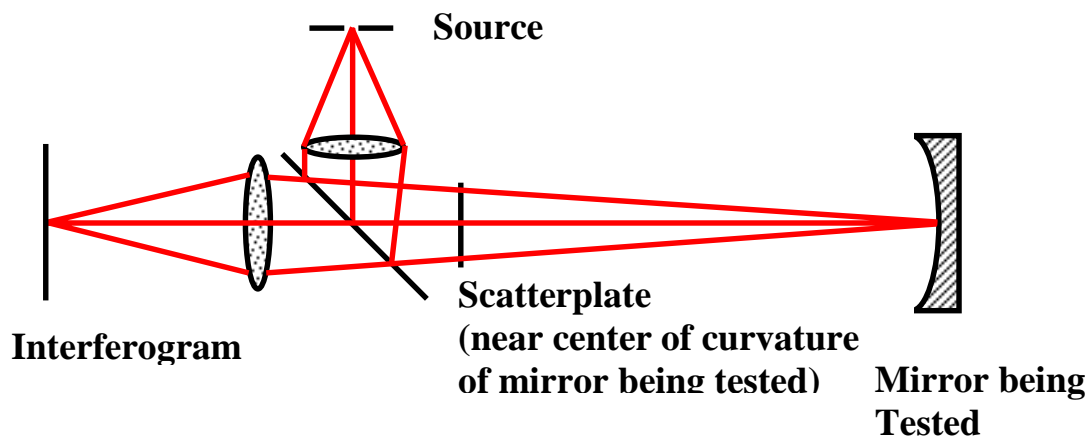

Fig. 8.2.6-1 Scatterplate interferometer for testing concave mirror.

Fig. 8.2.6-2 shows a photo of a scatterplate interferometer where the light source is a helium neon laser.
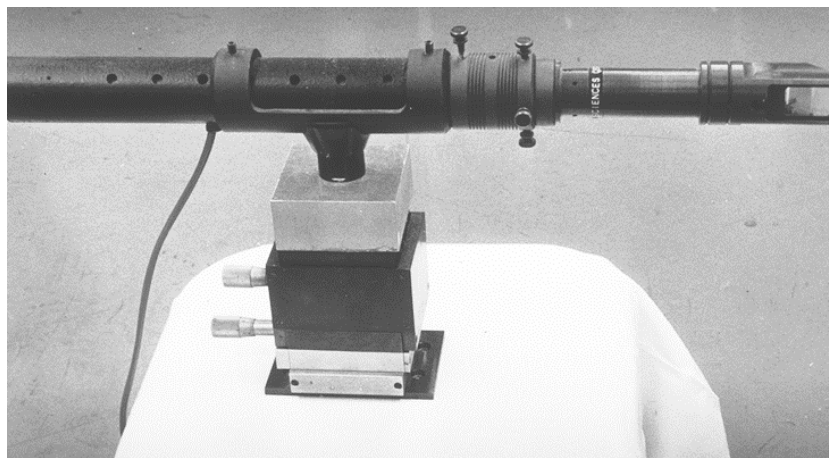

Fig. 8.2.6-2 Scatterplate Interferometer

The light transmitted through the scatterplate the second time can be divided into four categories dependent upon the influence of the scatterplate on the transmitted light: (1) unscattered-unscattered, (2) unscattered-scattered, (3)scattered-unscattered, and (4) scattered-scattered. The unscattered-unscattered light will produce a bright or hot spot in the interferogram, while the scattered-scattered beam will reduce the fringe contrast. If a laser source is used the scattered-scattered beam will give a high-frequency speckle pattern across the interferogram. The interference of the unscattered-scattered and scattered-unscattered beams gives fringes of constant contour that are just the same as those produced by a LUPI. Tilt in the interference fringes is introduced by lateral translation of the scatterplate, while longitudinal translation controls the amount of defocus. Fig. 8.2.6-3 shows 3 typical interferograms obtained using a scatterplate interferometer. The scatterplate interferometer was moved slightly between recording the three interferograms to change the amount of tilt and defocus.
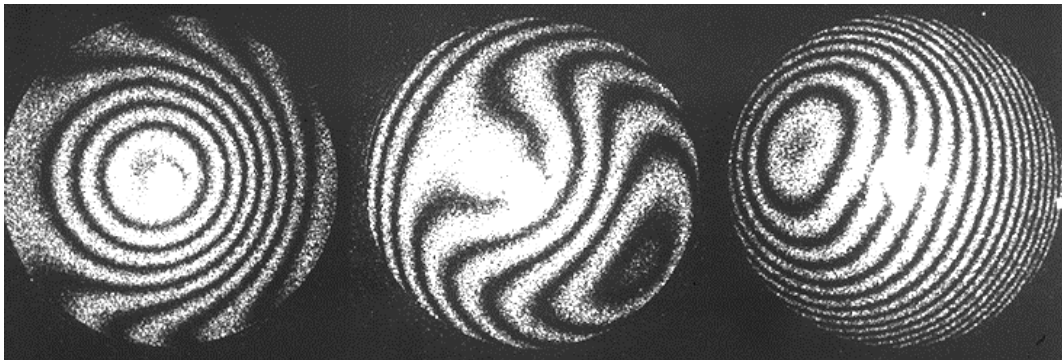

Fig. 8.2.6-3 Scatterplate interferograms of parabolic mirror.

The scatterplate interferometer is a very simple device, having a minimum of quality components. The most critical part of the instrument is the scatterplate itself, which can easily be made. The basic procedure for making a scatterplate is to expose a photographic plate to a speckle pattern produced by illuminating a piece of ground glass with a laser beam. Since the scatterplate must have inversion symmetry, two superimposed exposures to the speckle pattern must be made, where the plate is rotated 180° between the exposures. To ensure that the scatterplate illuminates the surface under test as uniformly as possible, during the making of the scatterplate the solid angle subtended by the illuminated piece of ground glass, as viewed from the photographic plate, should be at least as large as the solid angle of the surface under test, as viewed from the scatterplate during the test. After development, the photographic plate should be bleached to yield-a phase scatterplate. The exposure, development, and bleaching should be controlled so that the scatterplate scatters 10 to 20% of the incident light.

Fig. 8.2.6-4 shows a high magnification photograph of a scatterplate. This scatterplate was made for operation at a wavelength of 10.6 microns so the detail making up the scatterplate was large enough to easily observe through a microscope. Note the inversion symmetry of the structure making up the scatterplate.

Lateral Displacement Introduces Tilt
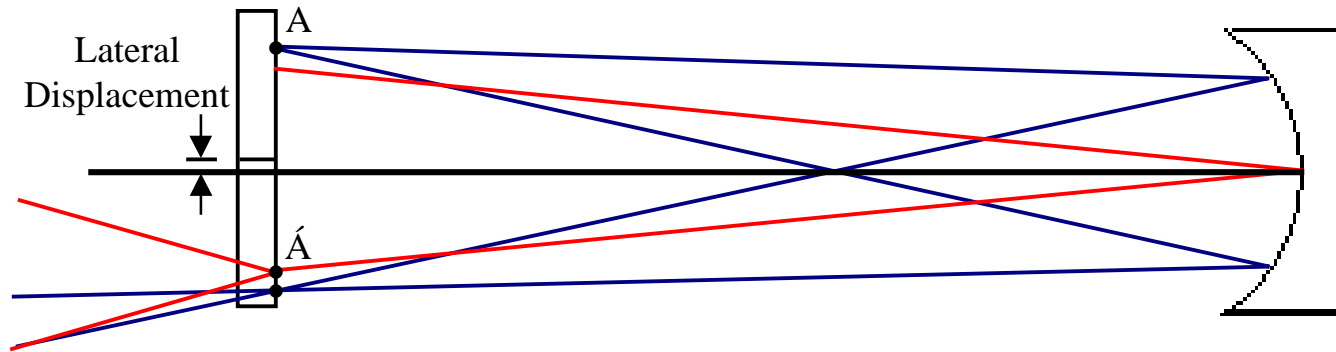
Longitudinal Displacement Introduces Defocus
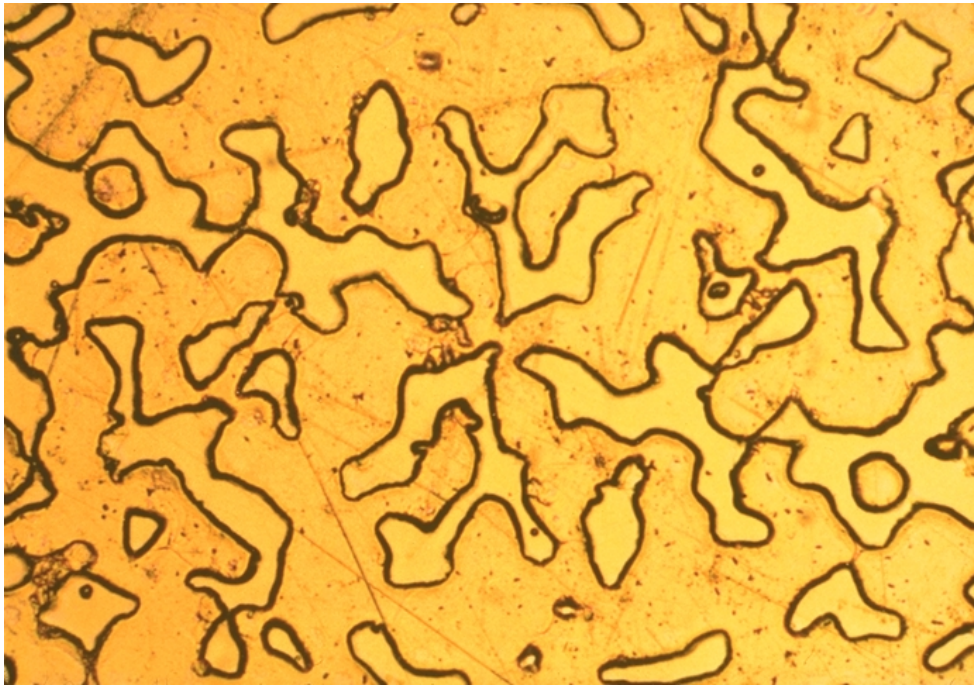
Center of curvature

A

Á

Image of A
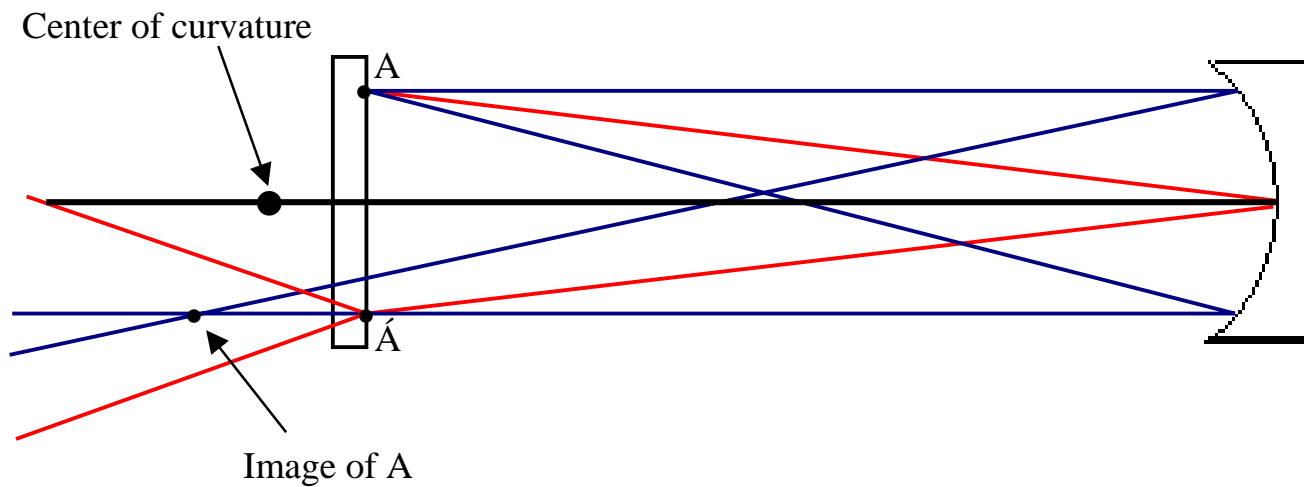
Fig. 8.2.6-4 High magnification photograph of a scatterplate.

The advantages of the scatterplate interferometer are that the instrument is simple and inexpensive, requires no accessory optics, and because the interferometer has a common path, it is less sensitive to vibration and turbulence. If an incoherent source is used as the light source, the coherent noise (extraneous fringes), normally associated with using a laser as the light source, is absent. The disadvantages are that the hot spot can cause a loss of fringes for a small portion of the interferogram and the twice-scattered beam will cause the interferogram to have somewhat lower contrast than can be obtained using a LUPI.

References

J.M. Burch, Nature (London) **171**, 889 (1953).

J.M. Burch, "Interferometry in Scattered Light," in *Optical Instruments and Techniques*, J.H. Dickson, Ed. (Oriel, London, 1970), p. 220.

J. M. Burch, "Scatter Plate Interferometry," J. Opt. Soc. Am. **52**, 600 (1962). (Abstract only).

R. M. Scott, "Scatter Plate Interferometry," Appl. Opt. **8**, 8531 (1969).

John Strong, "Concepts of Classical Optics", Appendix B (J. Dyson), (W.H. Freeman, San Francisco 1958), p. 377.

L. Rubin and J.C. Wyant, "Energy distribution in a scatterplate interferometer," J. Opt. Soc. Am. **69**, 1305 (1979).

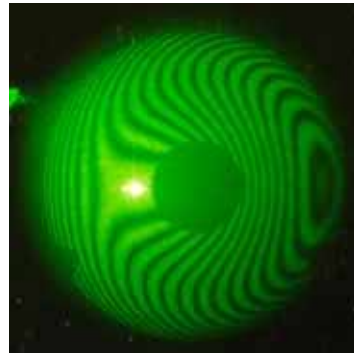L. Rubin and O. Kwon, "Infrared scatterplate interferometry," Appl. Opt. 19, 3219 (1980).

J. Huang, T. Honda, N. Ohyama, J. Tsujiuchi, "Fringe scanning scatter plate interferometer using polarized light," Optics Comm. **68**, 235 (1988).

D. Su and L. Shyu, "Phase shifting scatter plate interferometer using a polarization technique," J. Mod. Opt. **38**, 951 (1991).
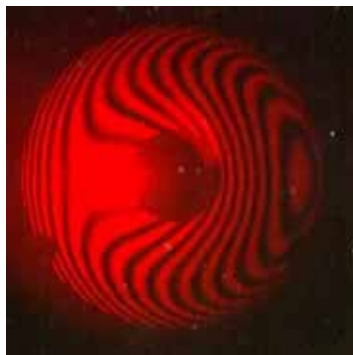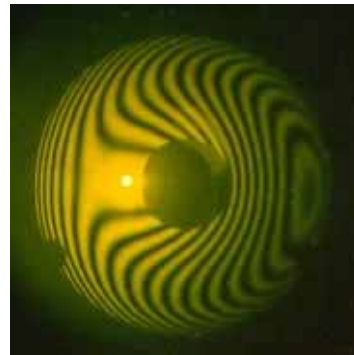
Scatterplate Interferograms
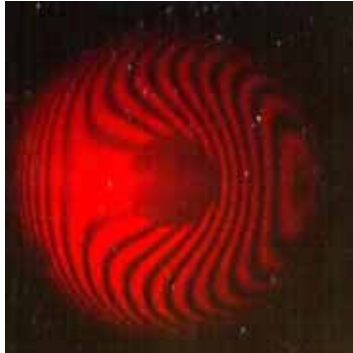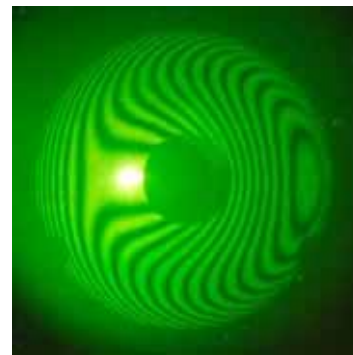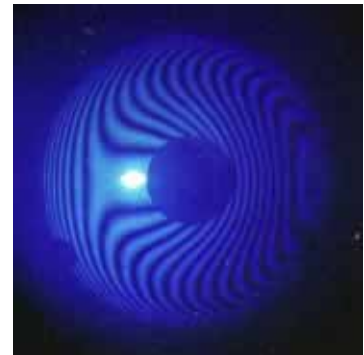

647.1 nm

520.8 nm

476.2 nm

All λ's except red

Absorptive scatterplate

568.2 nm, rotating ground glass

520.8 nm, rotating ground glass

476.2 nm, rotating ground glass
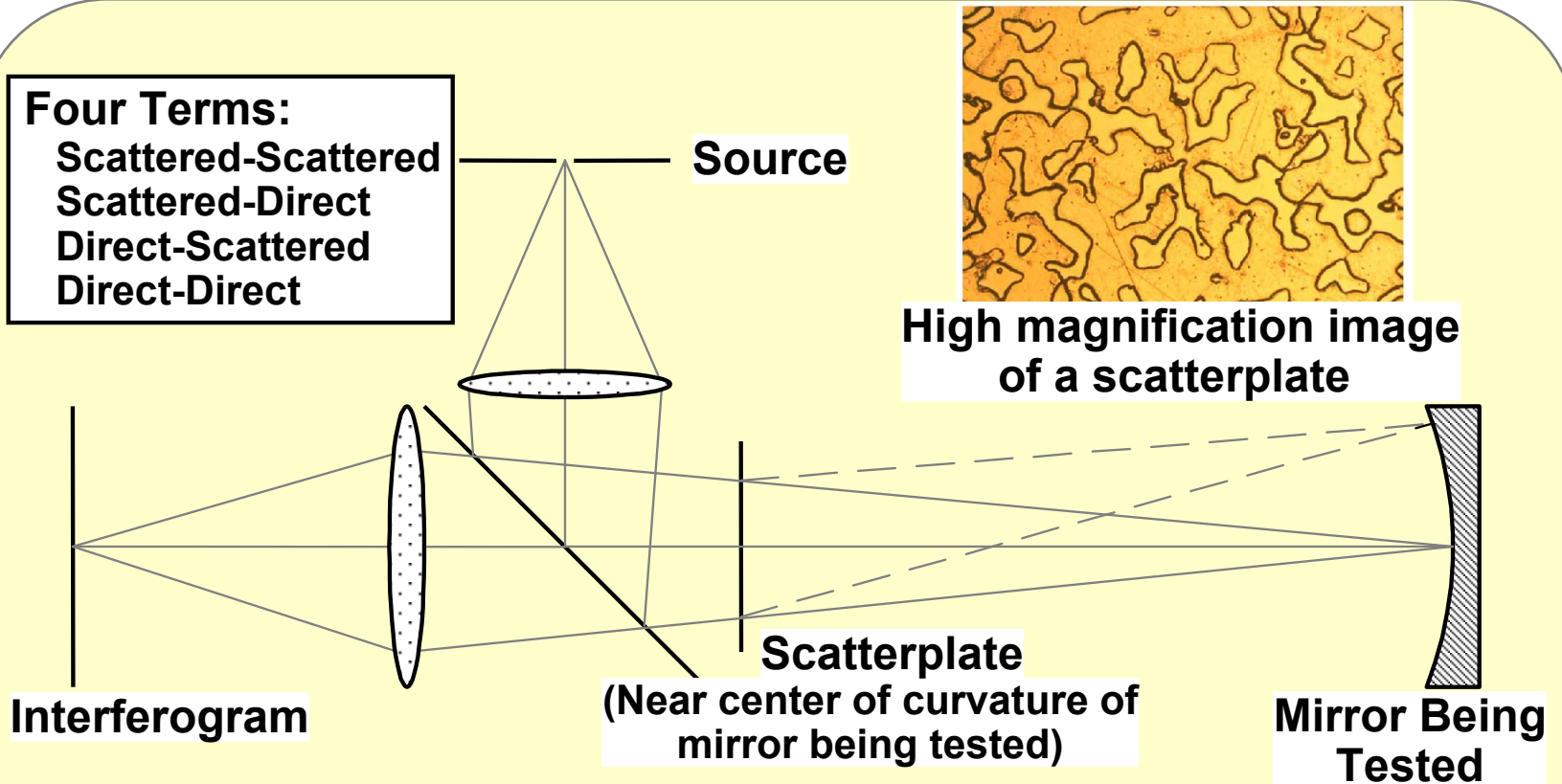
1998 - James C. Wyant

Phase-Shifting a Scatterplate Interferometer

Four Terms:
Scattered-Scattered
Scattered-Direct
Direct-Scattered
Direct-Direct

Source

High magnification image of a scatterplate

Interferogram

Scatterplate
(Near center of curvature of mirror being tested)

Mirror Being Tested

- Scatterplate has inversion symmetry

- Scatterplate is located at center of curvature of test mirror

- Direct-scattered and scattered-direct beams produce fringes

Separating Test and Reference Beams

- Difficult to separate spatially
  - Both test and reference traverse nearly the same path
- If test and reference have orthogonal polarization then phase-shifting is possible

Birefringent Scatterplate Makes Phase-Shifting Possible

- Scatterplate is made of calcite

- Oil matches ordinary index of calcite

- Scattering is polarization dependent

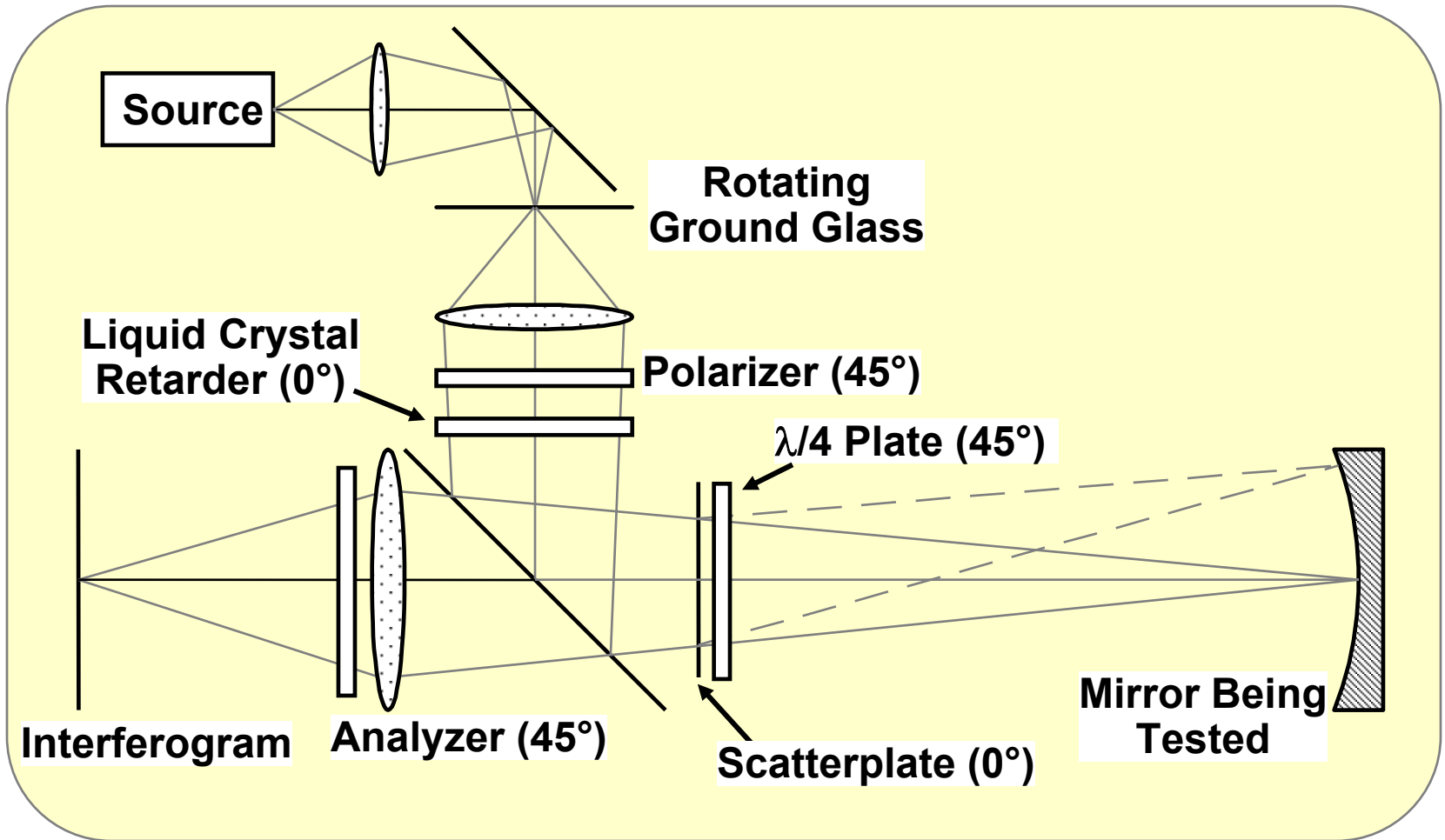Index Matching Oil

Calcite

Glass Slide
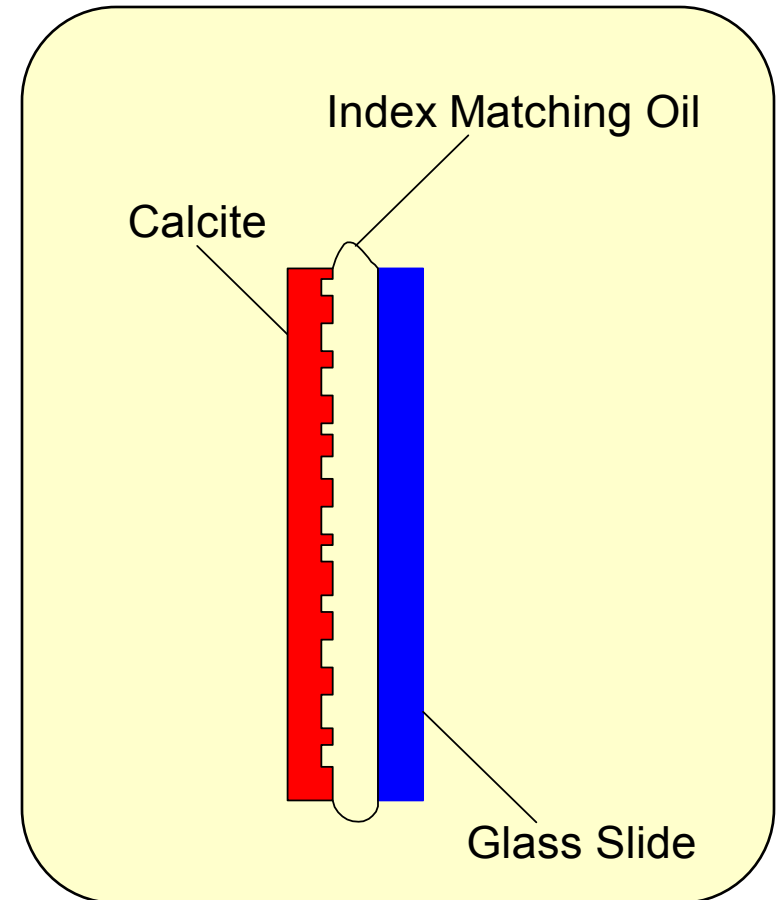
Scatterplate Production

Generated using six step process

1. Clean substrate
2. Spin coat with Photoresist
3. Expose
   - Holographic
   - Photomask
4. Develop
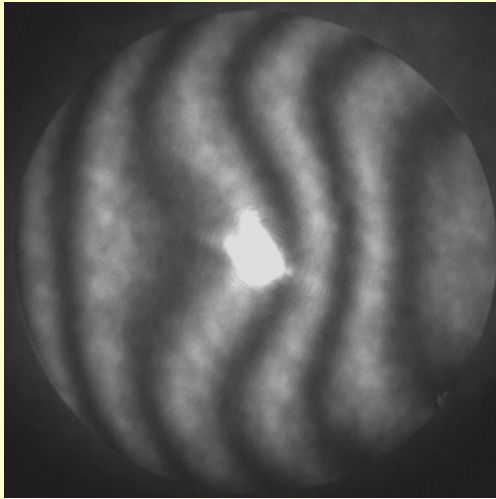5. Etch with 37% HCl Diluted 5000/1 in DI
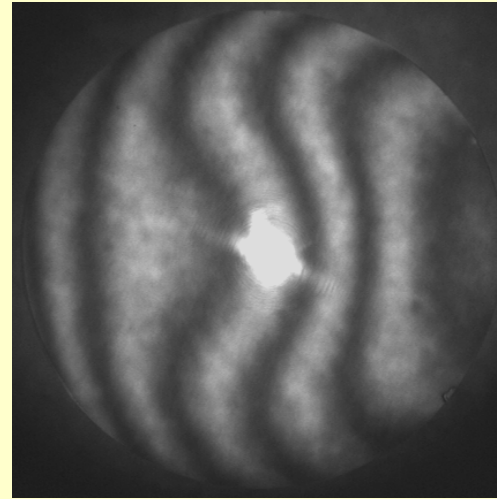6. Remove Photoresist
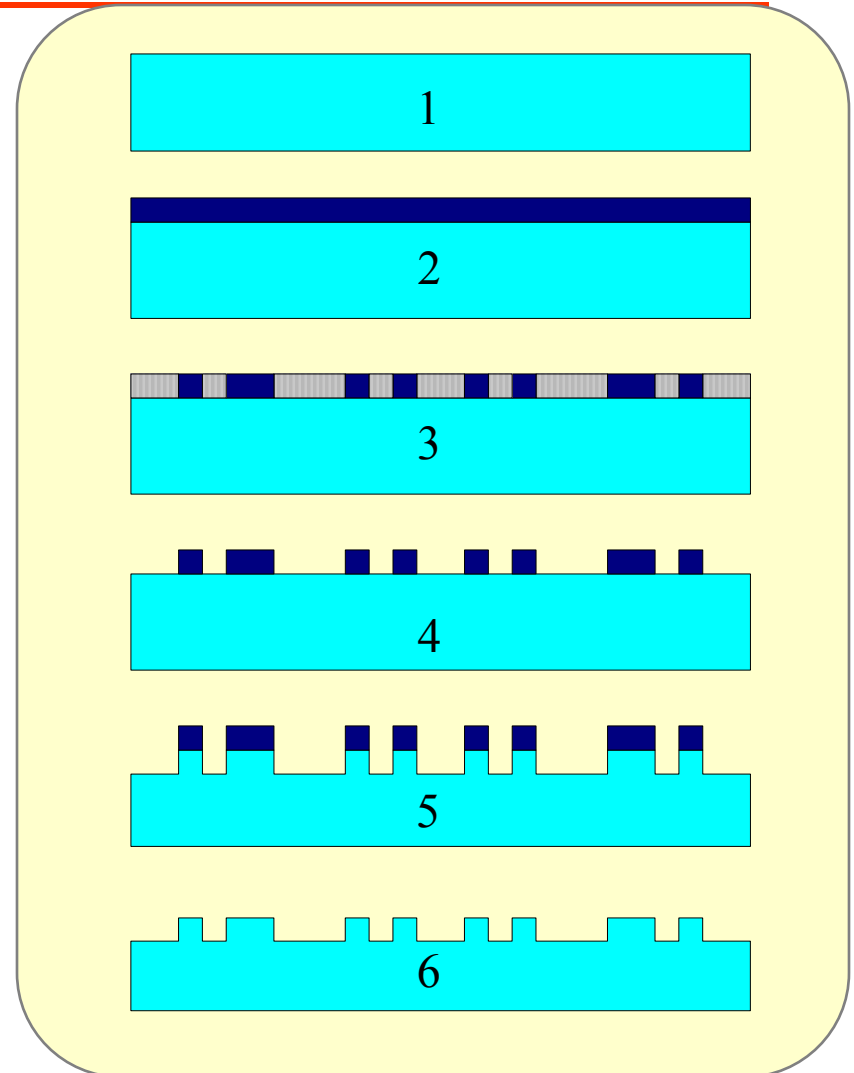
System Layout

Phase-Shifted Fringe Pattern

Frame 1

Frame 2

Frame 3
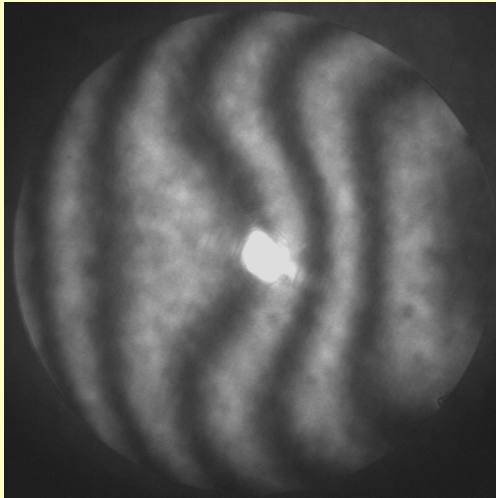
Frame 4
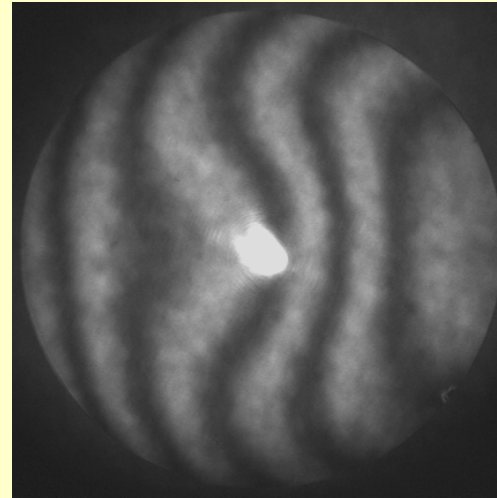
Surface Measurement Using Phase-Shifting Scatterplate Interferometer
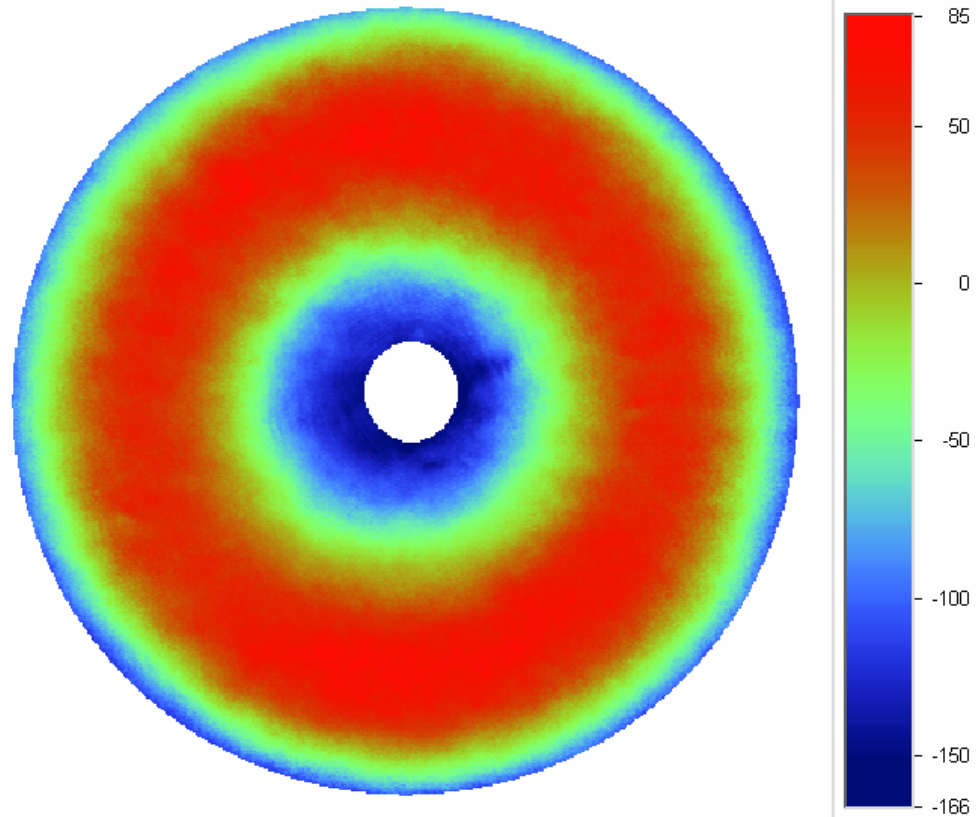
Measurement Comparison

Scatterplate
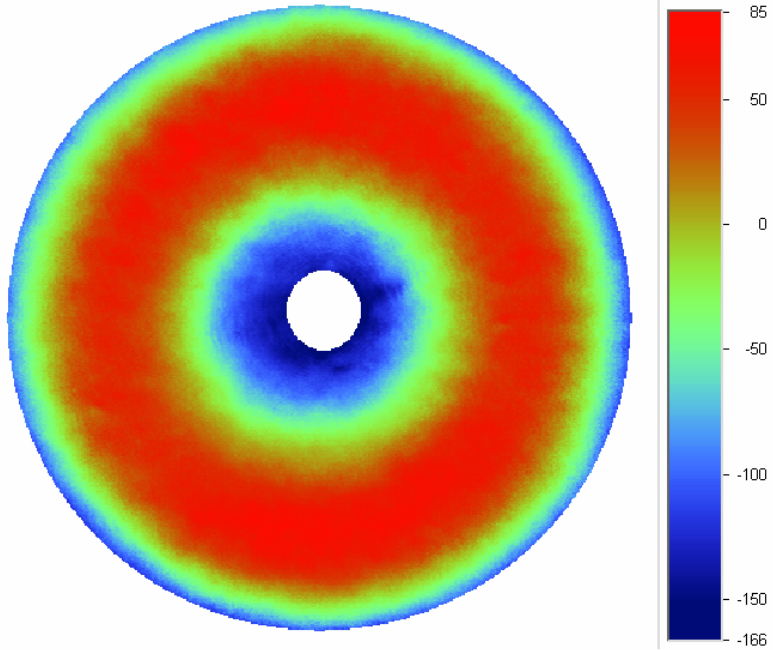
RMS = 0.008738 Waves

PV = 0.03750 Waves

WYKO 6000
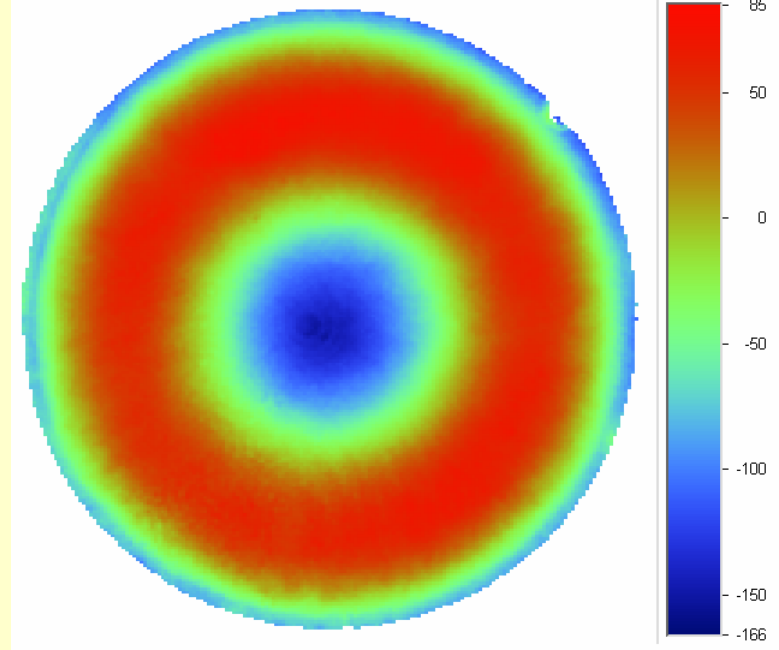
RMS = 0.008738 Waves

PV = 0.03405 Waves

Summary Phase-Shifting Scatterplate

- Birefringent scatterplate makes phase-shifting possible

- For this example

  - Accuracy ≈ 0.035 waves peak-to-valley

  - Repeatability ≈ 0.003 waves RMS

- Performance limited by liquid crystal retarder

8.2.7) Point-Diffraction Interferometer (Smartt)

The point diffraction interferometer (PDI) is basically a two-beam interferometer in which a reference beam is generated by the diffraction from a small pinhole in a semitransparent coating. The operation of the interferometer is described in the paper "Infrared point-diffraction interferometer".

The major disadvantage of the PDI is that the amount of light getting through the pinhole, and hence the amount of light in the reference beam, depends upon the position of the pinhole. That is, the contrast of the interference fringes depends upon the amount of aberration and upon the amount of tilt introduced into the interferogram. Typically, the amount of tilt in the interferogram can be changed by 5 to 7 fringes before the fringe contrast becomes unacceptable.

Smartt Point Diffraction Interferometer

Source

Lens under Test

Reference & Aberrated Wavefronts

PDI
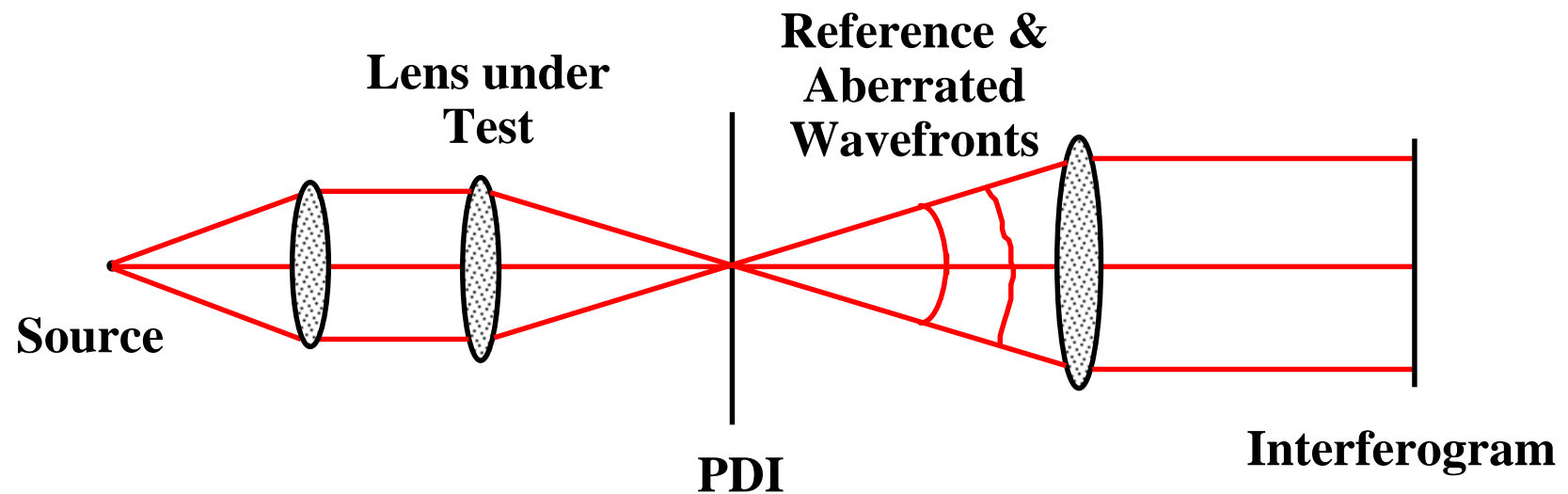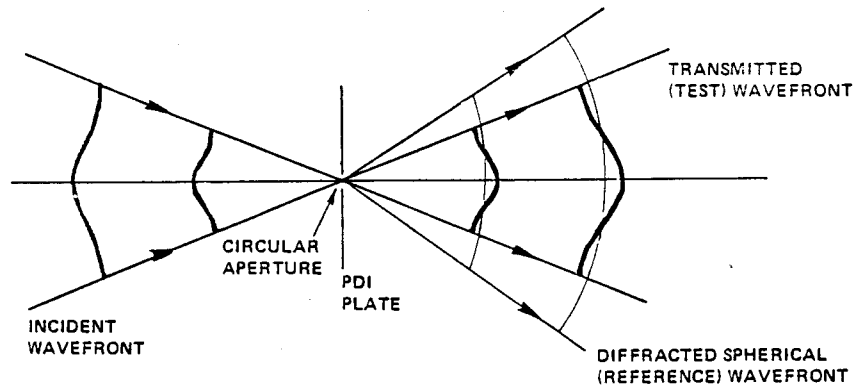
Interferogram

Operation of Smartt point diffraction interferometer.
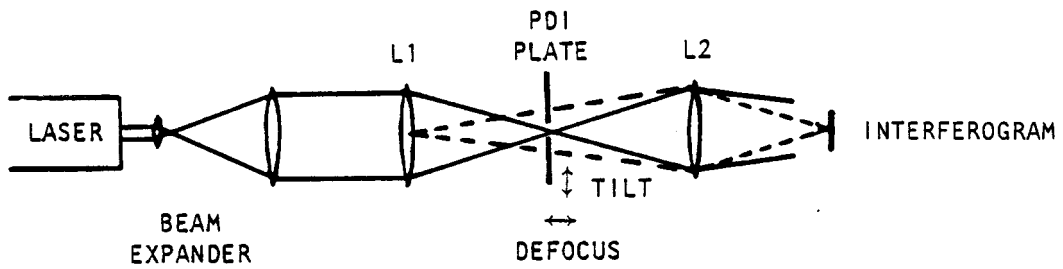
Point diffraction interferometer used to test a lens.
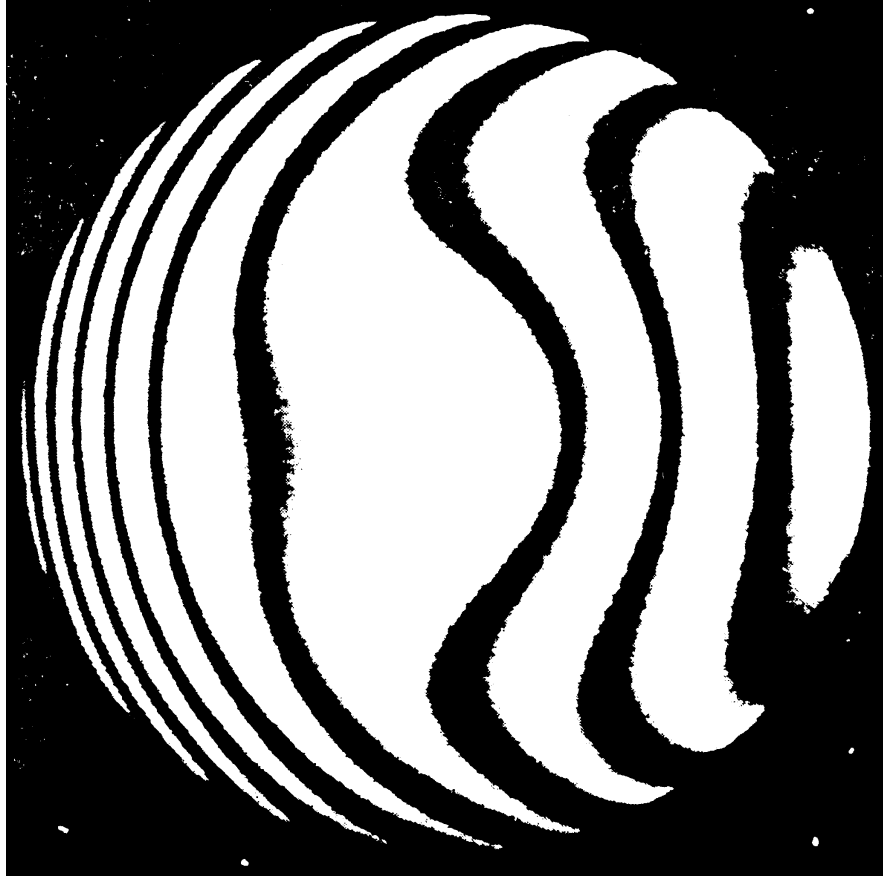
Typical interferogram obtained using PDI.

FROM
REMOTE LASER   LENS
UNDER TEST

CAMERA
LENS

PDI   INTERFEROGRAM
PLANE

FIGURE 7

CAMERA
LENS

COLLIMATING
LENS   LENS
UNDER TEST

PDI   INTERFEROGRAM
PLANE

LLICLE
AMSPLITTER

PDI

CAMERA LENS

INTERFEROGRAM PLANE

LENS
UNDER TEST   PLANE MIRROR

PELLICLE
BEAMSPLITTER

PDI

CAMERA LENS

INTERFEROGRAM PLANE

SURFACE
UNDER TEST
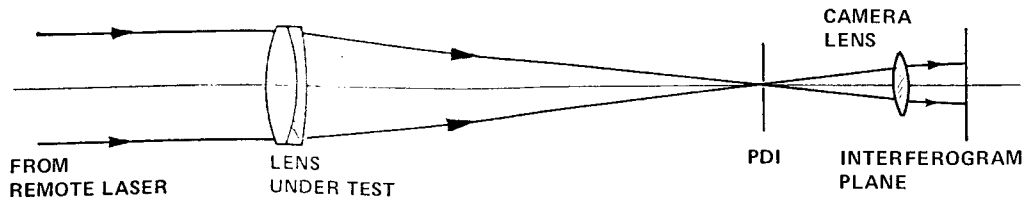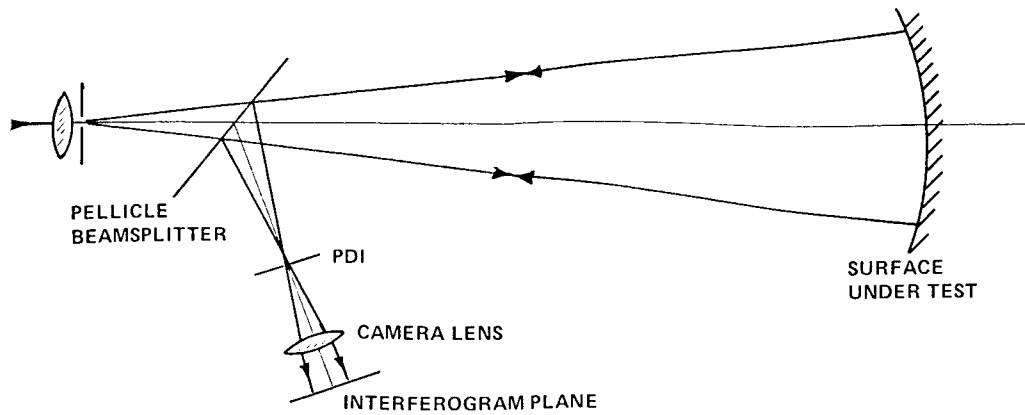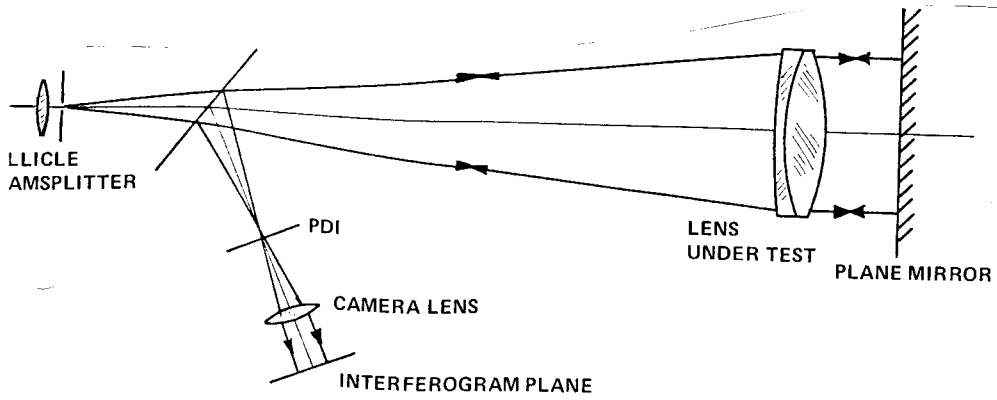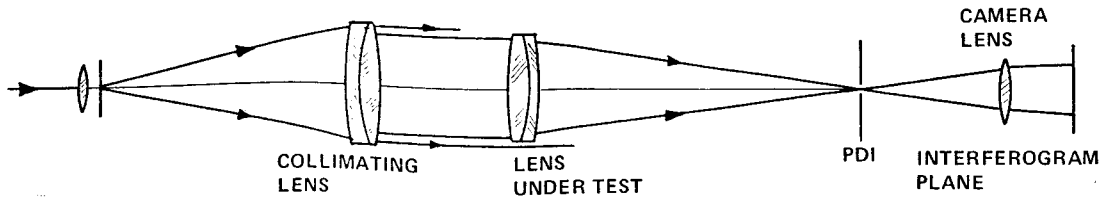
Typical test setups.

Point Diffraction Interferometer

Wavefront Measurement

diffracted wavefront "reference wave"

Incident wavefront

Transmitted "test wave"

Interferogram

Focusing lens

Point Diffractor
D = ½ Airy Disk Diameter
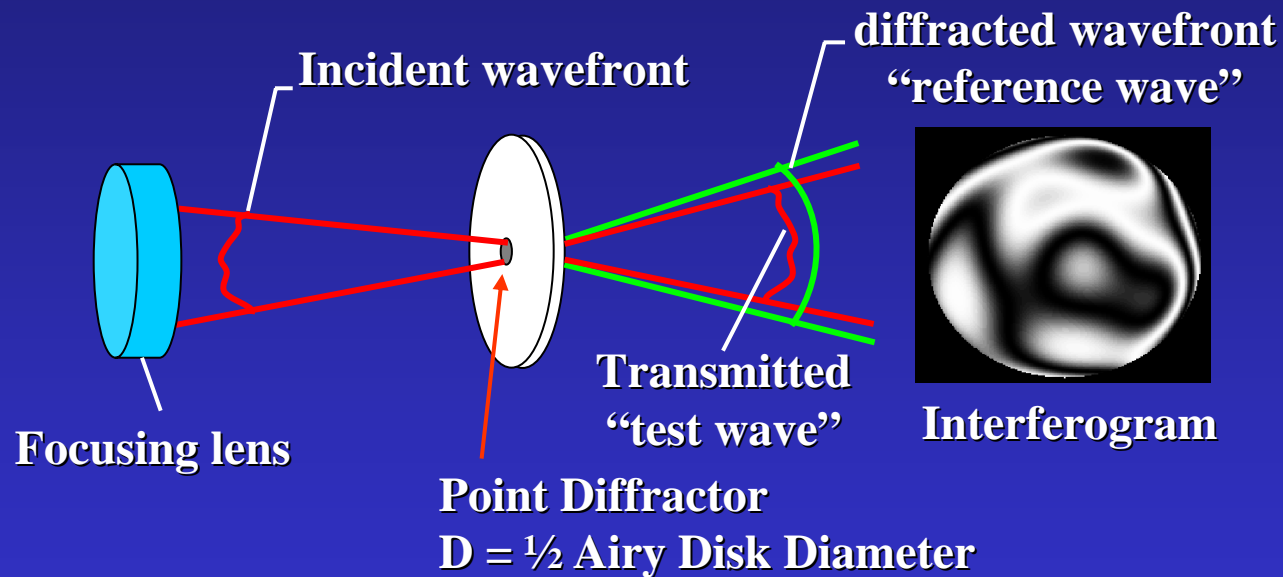
Generates "synthetic reference wave" from point diffracting element

Polarization PDI Construction

Finite Conducting Grids
"wire grid polarizer"

Clear center
Wire grid

substrate
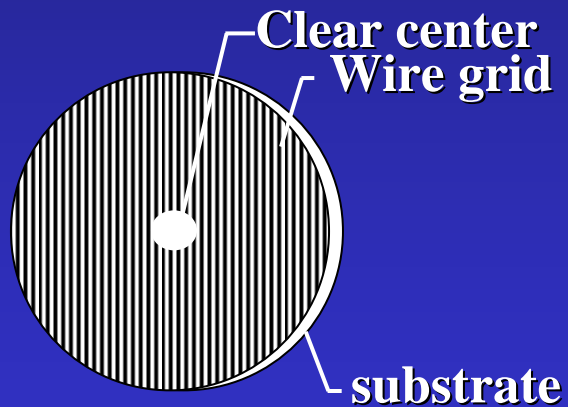
Requires pol. input light

Wire grid horizontal
Wire grid vertical

Substrate
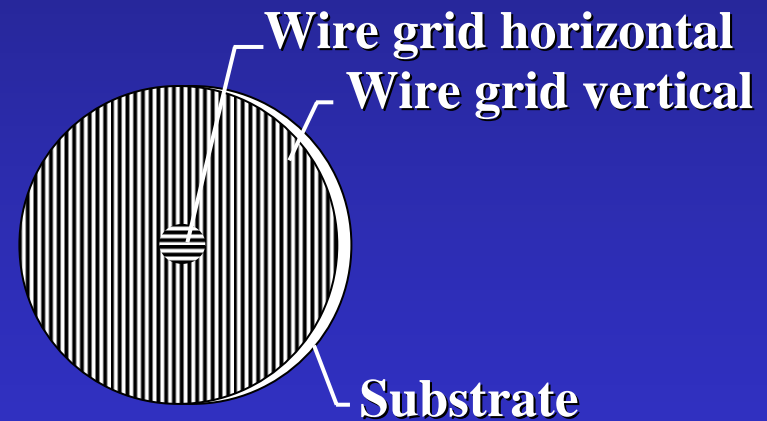
High contrast, any input pol.

Single Layer PDI Example
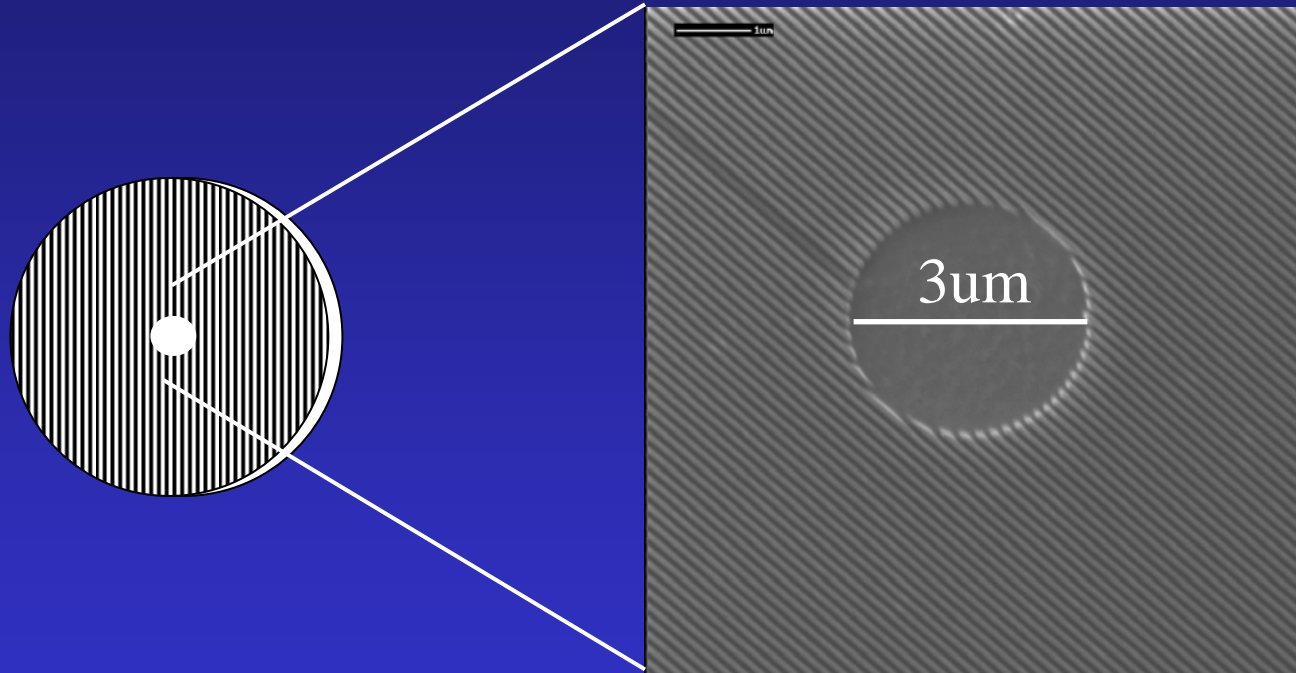
Focused Ion Beam Milling

Polarization PDI Multilayer Design
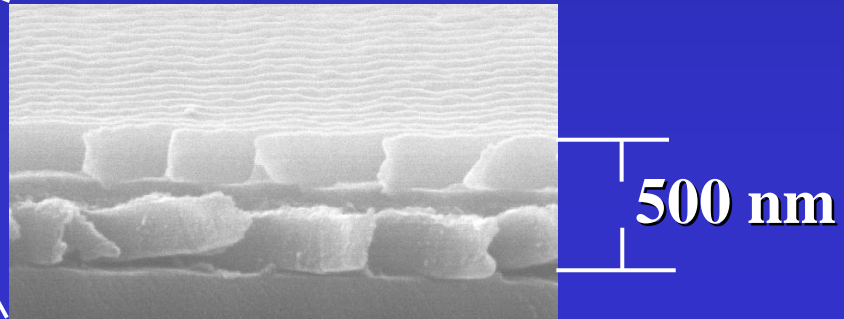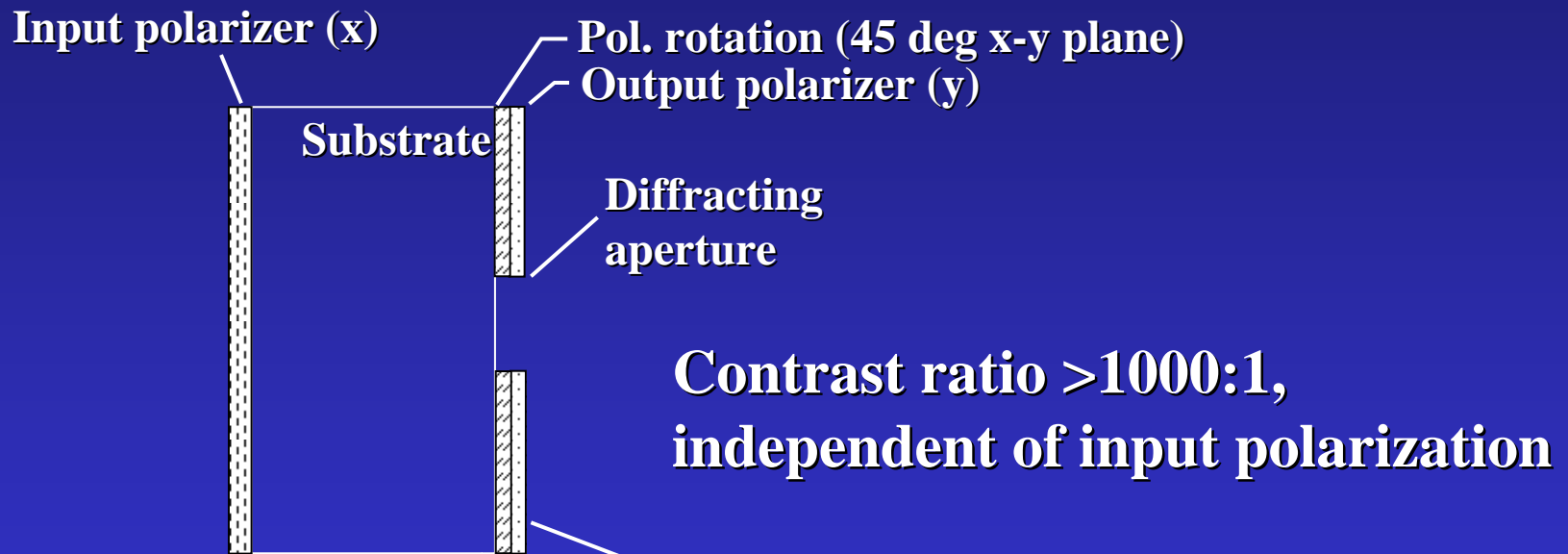
Instantaneous Phase-Shifting PDI
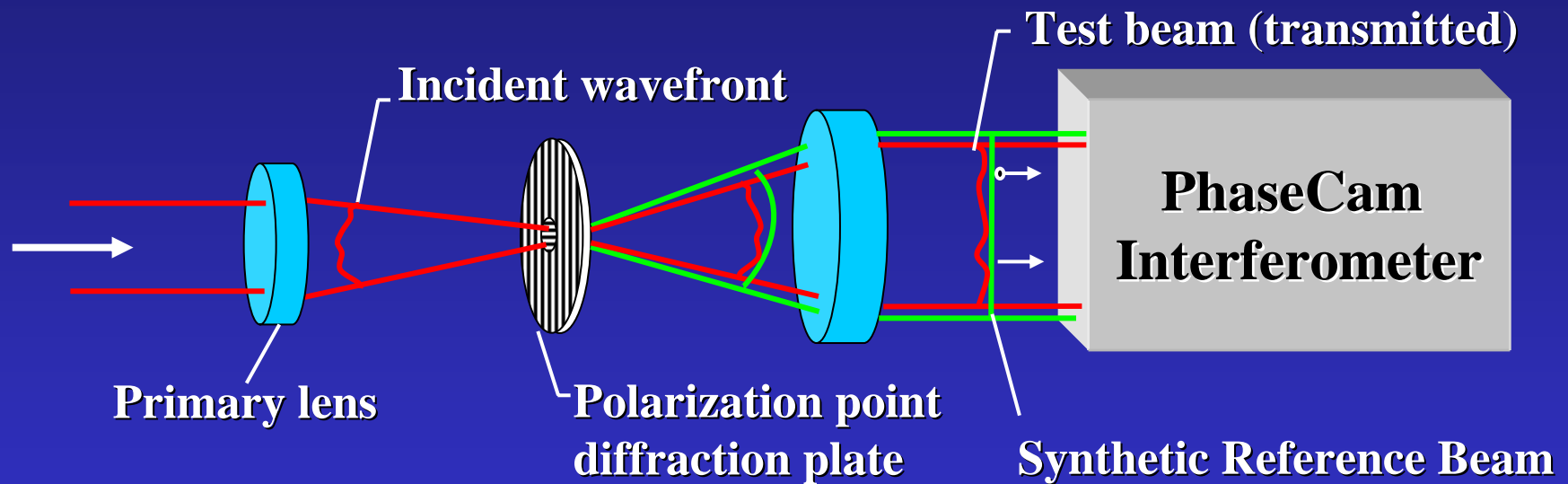
Synthetic reference wave is p-polarized
Transmitted test beam is s-polarized
Wavefront can be measured in a single shot!!!

Air Flow Measurement
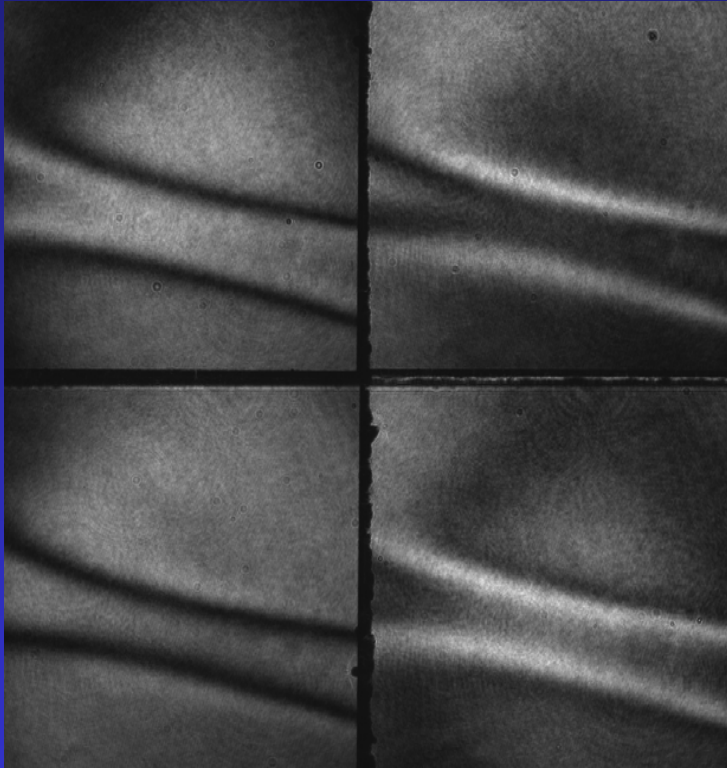
Simultaneous Interferograms
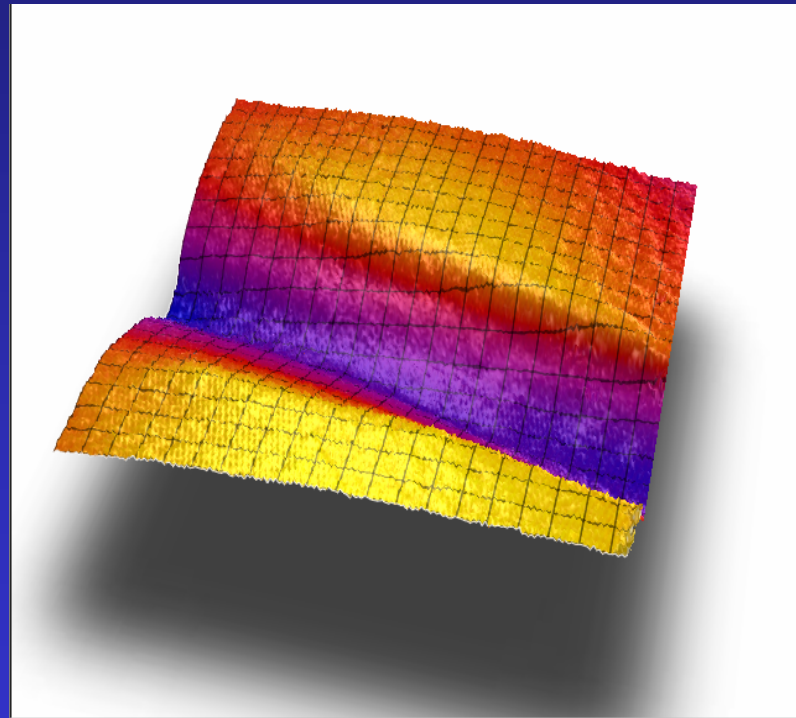
Phase Map

Sommargren Diffraction Interferometer

Short coherence length source

Optical fiber

Variable neutral density filter

Optic under test

Half-wave plate

Variable length

Microscope objective

CCD camera

Imaging lens

Polarizer

Interference pattern

Polarization beamsplitter

Quarter-wave plates

Computer system

PZT
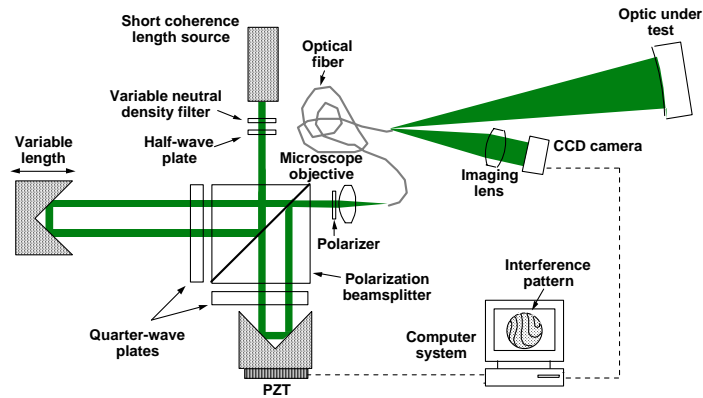
Phase Shifting Diffraction Interferometer (PSDI) configured to measure the surface figure of a concave off-axis aspheric mirror.

James C. Wyant

Detail of the diffracted and reflected wavefronts at the end of the fiber

Aberrated wavefront reflected from aspheric mirror

To aspheric mirror

Single mode optical fiber

Spherical wavefronts from fiber

Cladding

Core

Semi-transparent metallic film

To imaging lens

Aberrated wavefront reflected from end of fiber
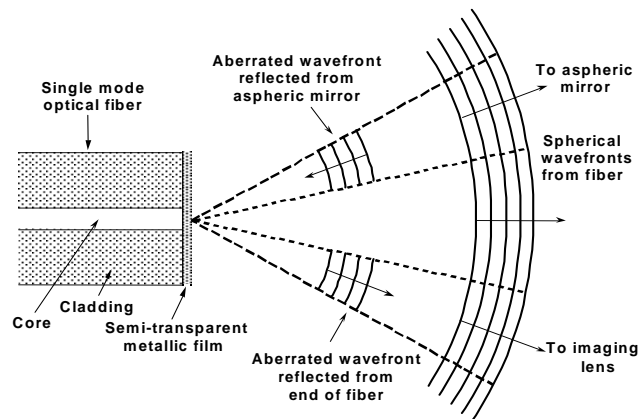
James C. Wyant

Cylindrical Surface Test

- Need cylindrical wavefront
  - Reference grating: Off-axis cylinder
  - Cylinder null lens: Hard to make

- Direct measurement - No modifications to interferometer

- Concave and convex surfaces

- Quantitative - phase measurement

Cylinder Null Lens Test Setup

Reference Surface

Collimated Beam

Cylinder Diverger Lens

Test Cylinder (Angle Critical)
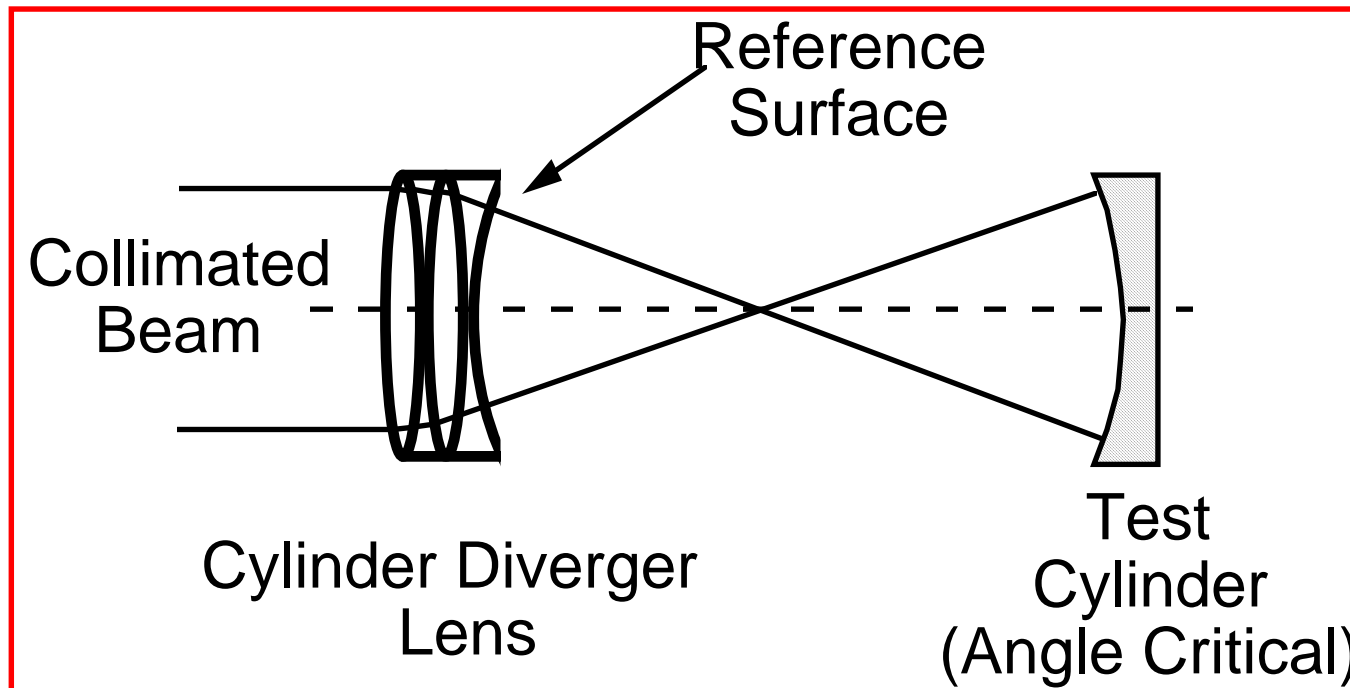
Cylinder Grating Test Setup

Transmission Flat

Reference Surface

Collimated Beam

Cylinder Grating

1st Order From Grating

Test Cylinder (Angle Critical)

Grating Lines
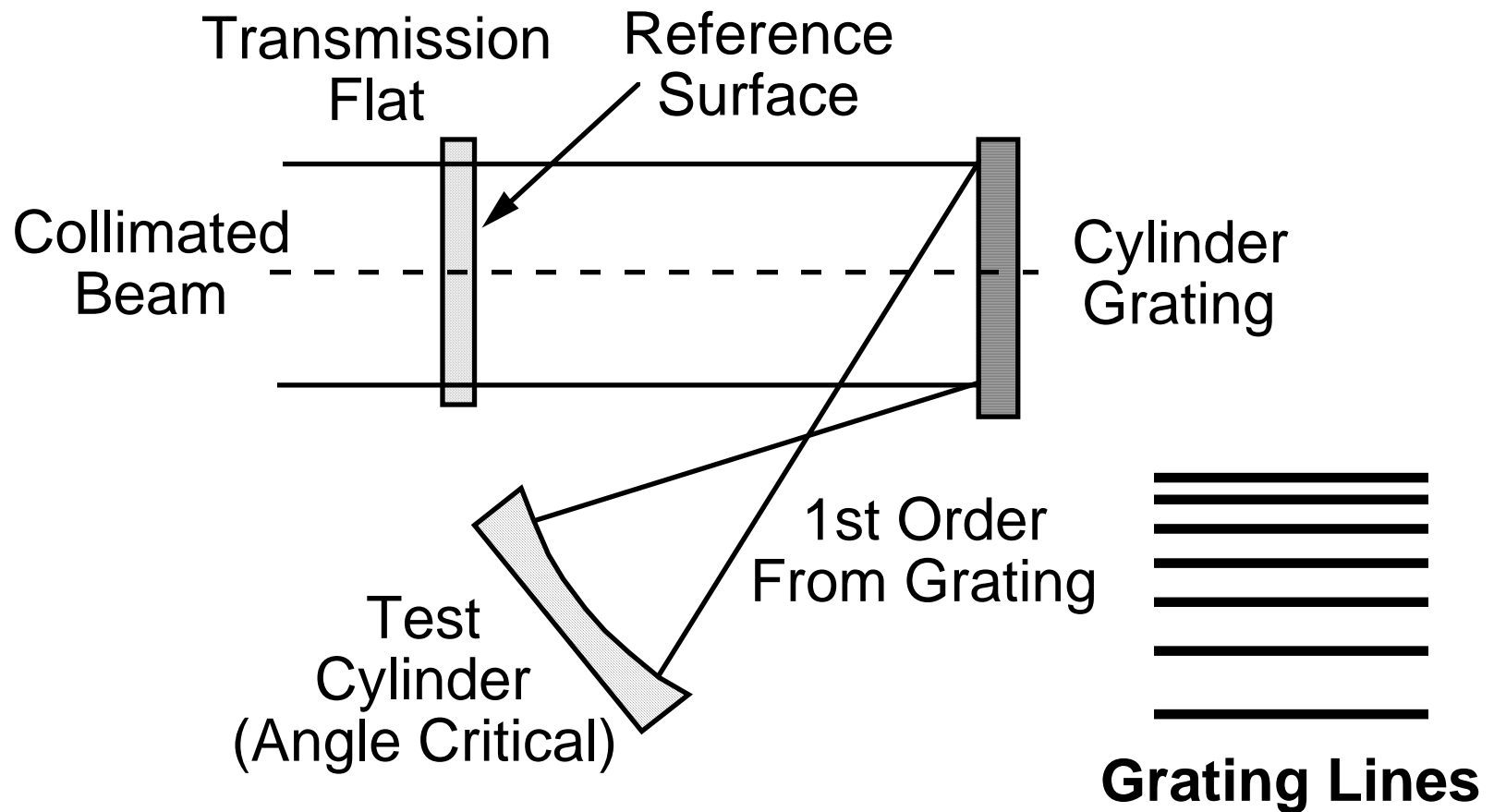
8.2.10) Star Test

Ref: Chapter 11 of Malacara

The careful visual examination of the image of a point source formed by a lens being evaluated is one of the most basic and important tests that can be performed. The interpretation of the image in terms of aberrations is to a large degree a matter of experience, and the visual examination of a point image should be a dynamic process. The observer probes through focus and across the field to determine the type, direction, and magnitude of aberrations present. For ease of carrying out the test, the magnifying power should be such that the smallest significant detail subtends an easily resolvable 10 to 15 minutes of arc at the eye. It is also important that the numerical aperture of the viewing optics is large enough to collect the entire cone of light from the optics under test.

If the lens being tested is perfect, the image of a point source as seen at best focus is called the Airy disk. The Airy disk consists of a bright circular core surrounded by several rings of rapidly diminishing brightness. The diameter of the central core is equal to 2.44λf#, where f# is the f/number of the converging light beam. Note that in the visible, the diameter of the central core is approximately equal to the f# in microns. The central core contains approximately 84% of the total amount of light, while the total amount of light contained within the first, second, and third rings is approximately 91%, 94%, and 95%, respectively. If the microscope is moved back and forth along the axis, the image will be seen to go in and out of focus. The change in the pattern is rather complex, consisting first of a redistribution of light from the core to the rings, then with larger focus shifts the diameter of the image will appear to grow. A perfect image will appear totally symmetrical on opposite sides of focus as shown in Fig. 8.2.10-1.

Spherical aberration, coma, and astigmatism are also easily observed using the star test. The presence of spherical aberration is most easily inferred by examination of the symmetry of the image through focus. As one focuses on the image, starting from well inside the marginal image plane and moving toward paraxial focus, the following set of images shown in Fig. 8.2.10-3 is noted for undercorrected spherical. First, a diffuse, fairly uniform blur is seen. As the region of the marginal focus is approached, the beginning of the outer spherical caustic is reached. Here, a "hollow" or ring image is observed. Next, the ring diminishes in size and intensity and gives way to a core with a rather bright set of surrounding diffraction rings. Eventually, the size of this structure reaches a minimum and then becomes a small, intense core surrounded by a diffuse halo. Beyond the paraxial plane a growing diffuse flare is observed. The best focus (minimum spot size) occurs at ¾ the distance from paraxial to marginal focus. The minimum spot size is ¼ the spot size at paraxial focus.

Off-axis images are complex. Almost always, a mixture of coma and astigmatism of various orders is obtained. For third-order coma, the image looks much as indicated in Fig. 8.2.10-5, while the line foci for third-order astigmatism appears as indicated in Fig. 8.2.10-6. Fig. 8.2.10-7 shows the diffraction pattern for third-order astigmatism in the neighborhood of the circle of least confusion.

It is useful to obtain a rough estimate of the geometrical spot size produced by the different aberrations. Let ΔW be the maximum aberration for third-order spherical, coma, and astigmatism and f# be the f/number of the converging light beam. At paraxial focus, the blur radius ε_y, for third order spherical is given by

$$\varepsilon_y = 8f\#\Delta W_{sph}$$

The minimum radius of the blur due to third-order spherical would be ¼ of this.

The tangential coma, ε_y, is given by

$$\varepsilon_y = 6f\#\Delta W_{coma}$$

The sagittal coma is 1/3 this value and the width of the coma image is 2/3 of this.

The length of the line focus for astigmatism is given by

$$2\varepsilon_y = 8f^{\#}\Delta W_{ast}$$

The blur for astigmatism halfway between the sagittal and tangential focus would be ½ of this value.

Therefore, the minimum spot diameter for third-order spherical, the width of the coma image (2/3 the tangential coma), and the diameter of the blur for astigmatism that falls halfway between the sagittal and tangential focus are all given by

$$\boxed{d = 4f\#\Delta W}$$

where again ΔW is the maximum wavefront aberration due to third-order spherical, coma, or astigmatism at the edge of the pupil.

It is of interest to look at the ratio of geometrical blur to the Airy disk diameter.

$$\frac{Geometrical\ Blur\ Diameter}{Airy\ Disk\ Diameter} = \frac{4f\#\Delta W}{2.44\lambda f\#} = 1.64\left(\frac{\Delta W}{\lambda}\right)$$

That is, the ratio of the geometrical blur diameter to the Airy disk diameter is approximately equal to 1.64 times the amount of aberration in units of waves.

The star test is very useful for detecting chromatic aberration. The testing is carried out by observing the color changes in the image as the focal position is varied toward and away from the lens. In a perfectly apochromatic system a symmetrical "white" image is obtained for all focal positions. Chromatic aberration provides an image whose color is a function of focal position. In moving away from the lens through the paraxial focal plane, a sequence of images is observed. Well away from focus, a white flare is

observed. As the blue focus is reached, the color balance is seen to change as blue light appears to be removed from the flare and is concentrated in a core. Farther away from the lens a similar color effect is observed as the foci for green and red are reached. For overcorrected color, the colors appear in the opposite order.

The chromatic errors in an off-axis image are most spectacular in visual testing. The lateral separation of the images in red and blue light gives directly the amount of lateral chromatic aberration. If the red image is found to lie at a greater distance from the axis than the blue image, negative or undercorrected lateral color is present, while for overcorrected lateral color, the blue image is a greater distance from the axis than the red image.

The following pictures are from "Atlas of Optical Phenomena" by Cagnet, Francon, and Thrierr.
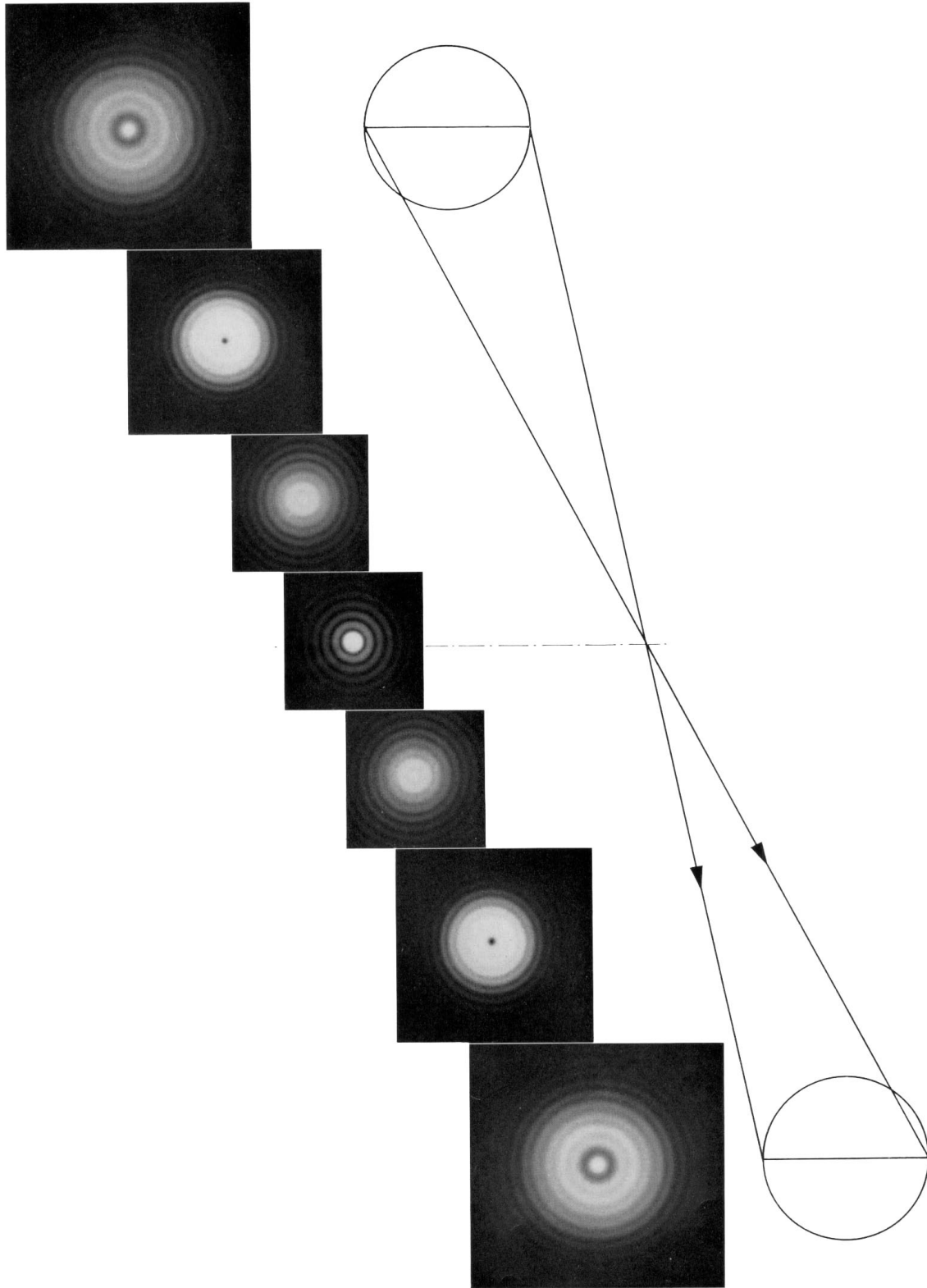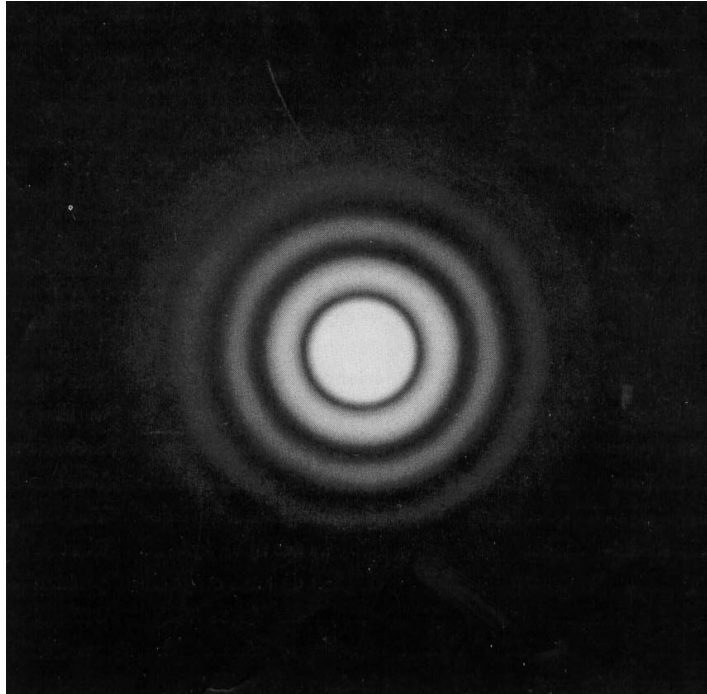
Fig. 8.2.10-1. Diffraction by a circular aperture as a function of defocus for no aberration

Airy Disk
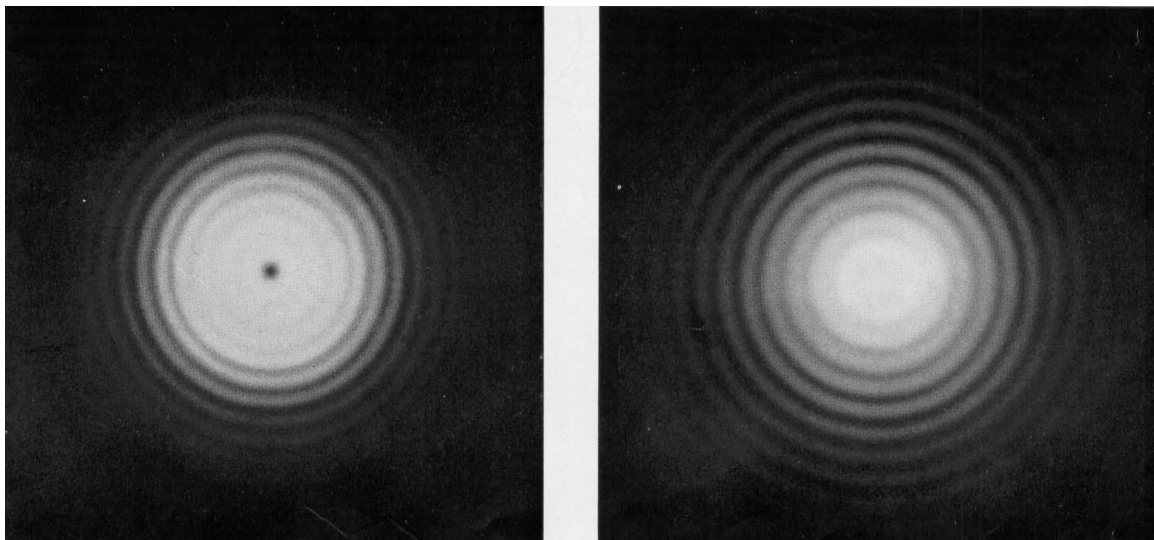
1 wave defocus   Less than 1 wave defocus

Fig. 8.2.10-2. Diffraction by a circular aperture in the presence of defocus.
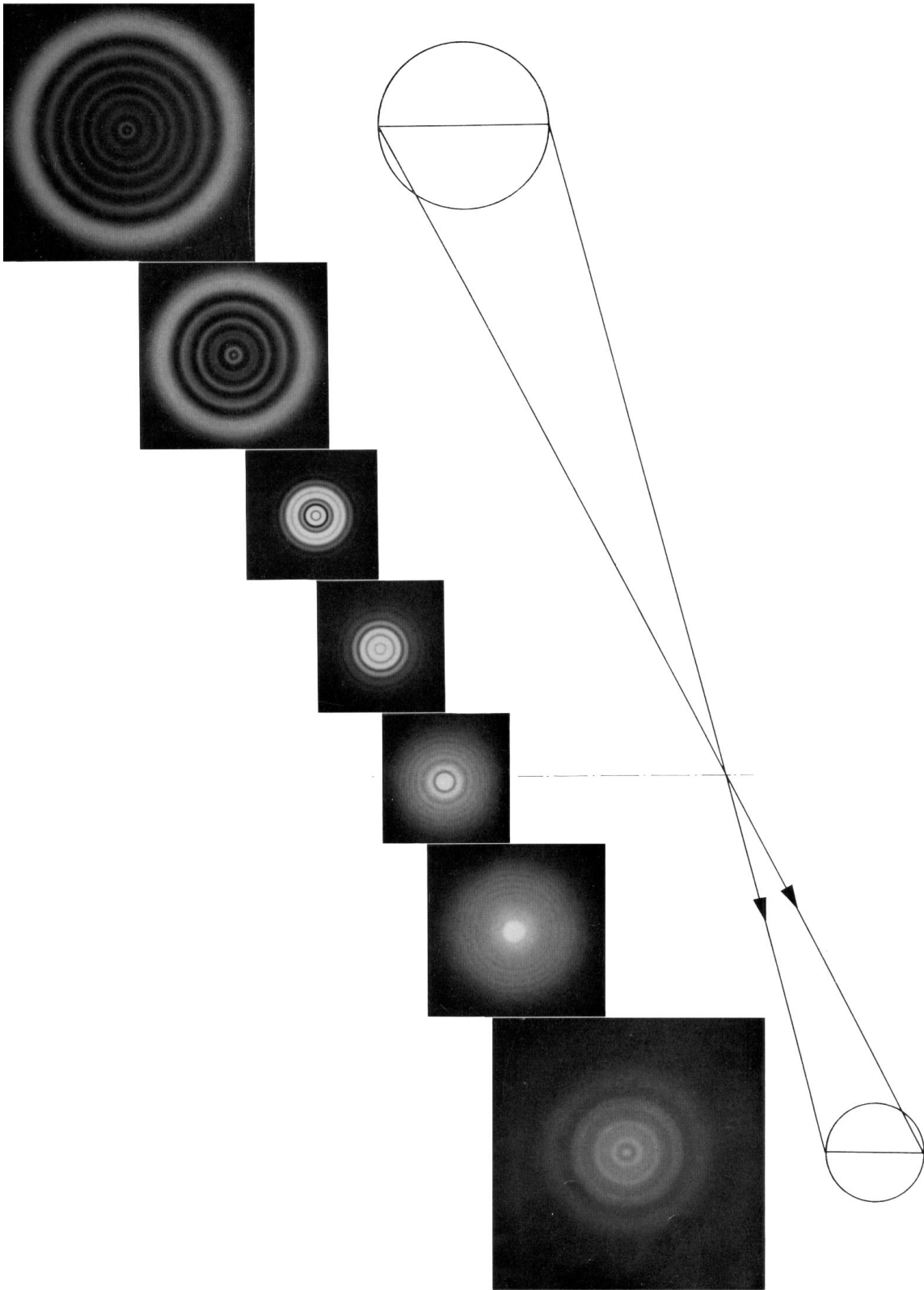
Fig. 8.2.10-3. Diffraction by a circular aperture as a function of defocus for third-order spherical aberration
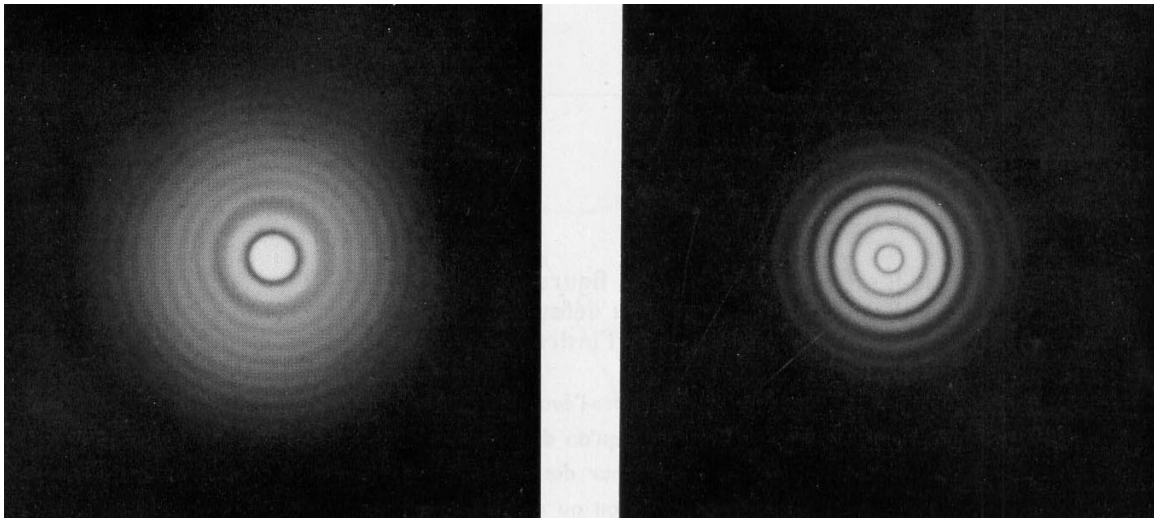
Paraxial Focus   Small distance inside paraxial focus
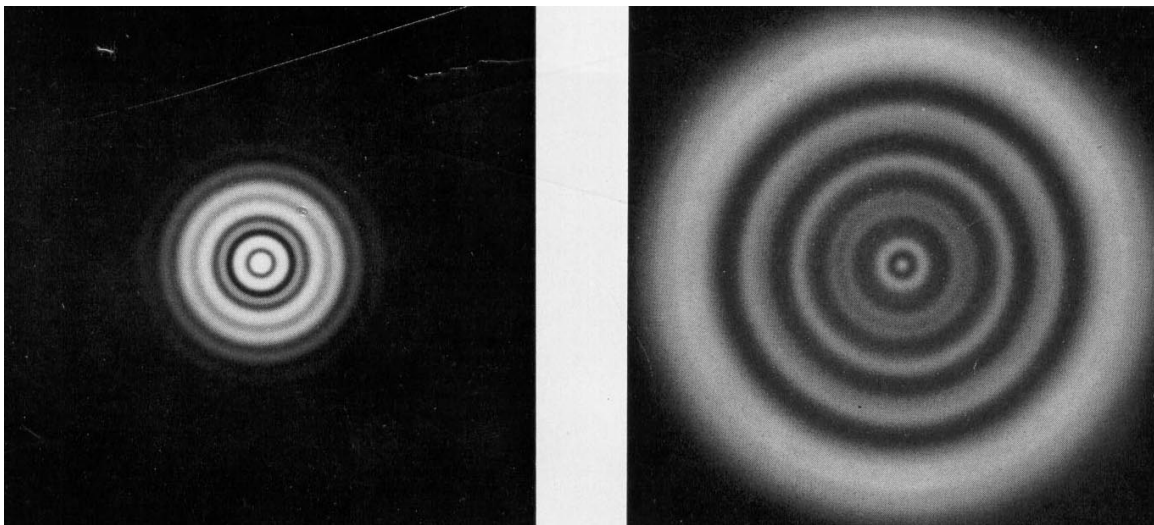
Moderate distance from marginal focus   Immediate neighborhood of marginal focus

Fig. 8.2.10-4. Diffraction by a circular aperture in the presence of third-order spherical aberration.

6 λ

2.5 λ   1 λ
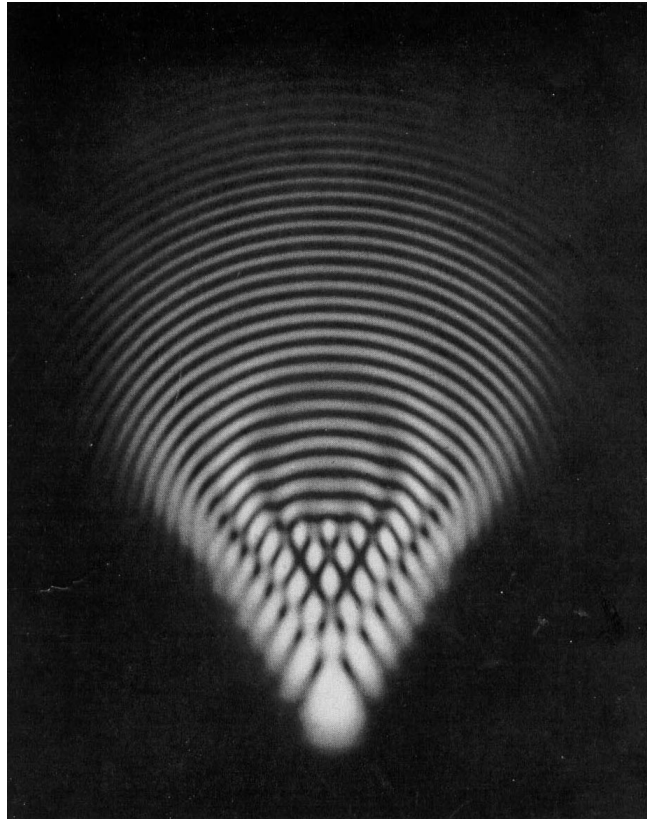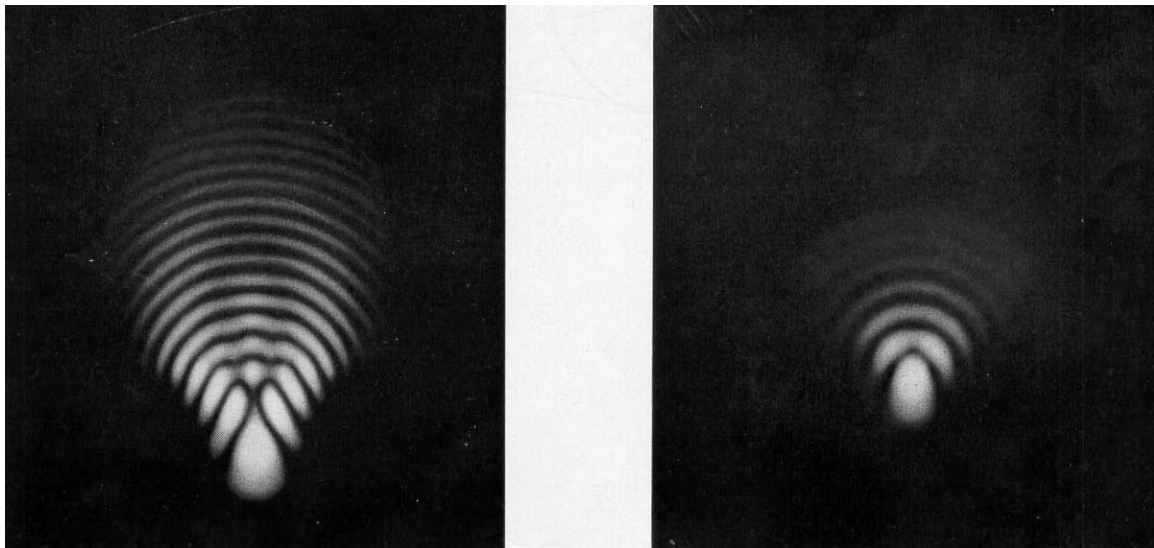
Fig. 8.2.10-5. Diffraction by a circular aperture in the presence of third-order coma.

7 λ

1.5 λ   0.23 λ
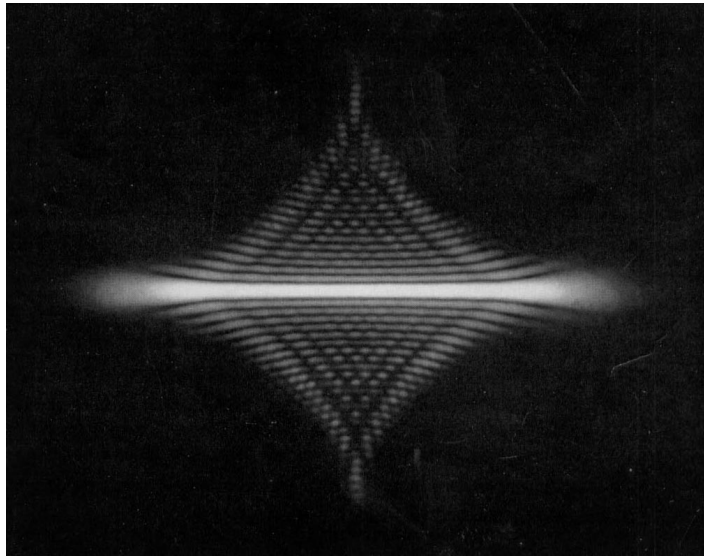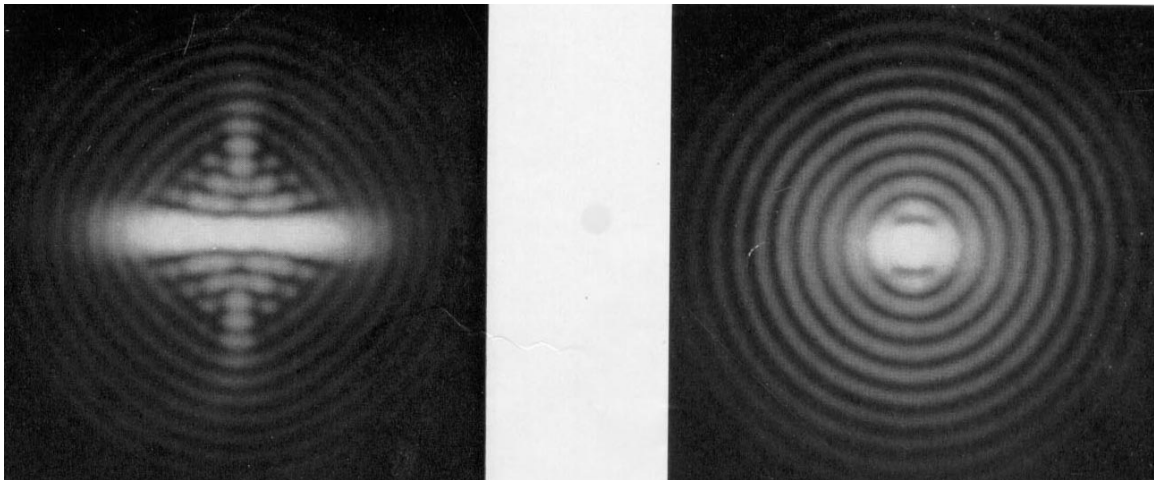
Fig. 8.2.10-6. Diffraction by a circular aperture in the presence of astigmatism.

7 λ

1.6 λ   0.23 λ

Fig. 8.2.10-7. Diffraction by a circular aperture in the presence of astigmatism in the neighborhood of the circle of least confusion.

Shack-Hartmann Test

The Shack-Hartmann test is essentially a geometrical ray trace that measures angular, transverse, or longitudinal aberrations from which numerical integration can be used to calculate the wavefront aberration.

Figure 1 illustrates the basic concept for performing a classical Hartmann test. A Hartmann screen, which consists of a plate containing an ar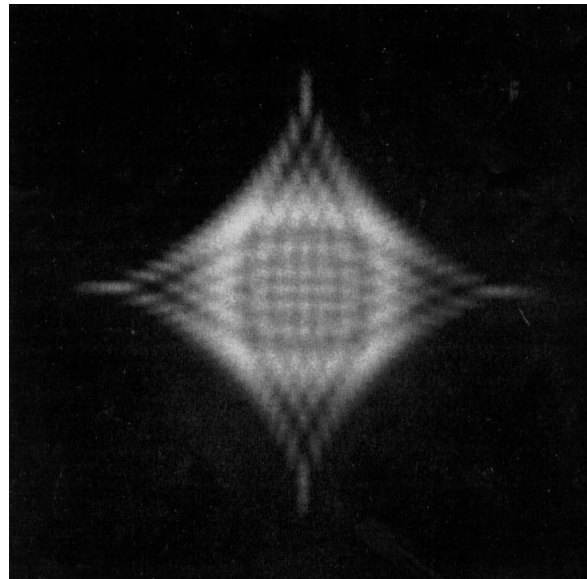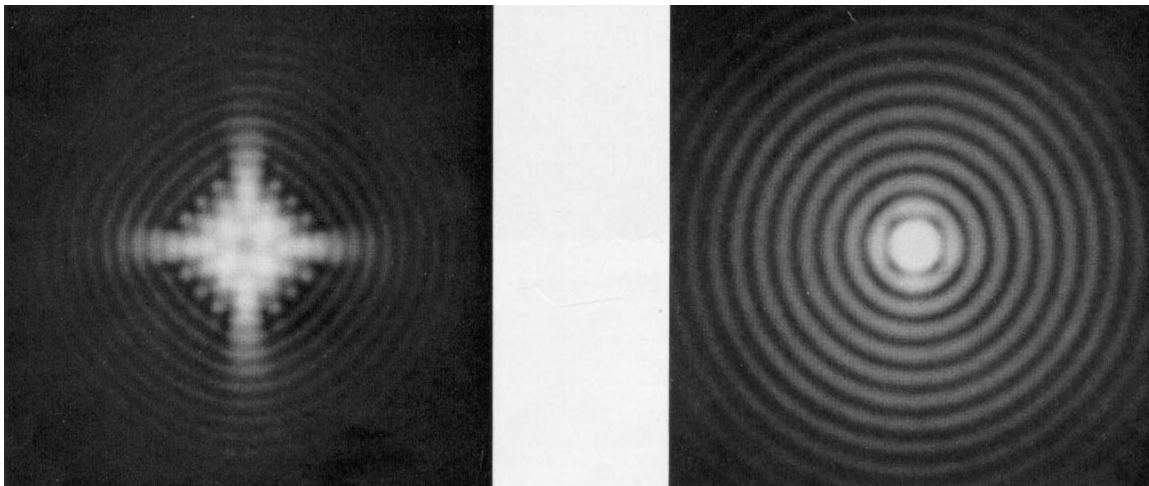ray of holes, is placed in a converging beam of light produced by the optics under test. One or more photographic plates or solid-state detector arrays are placed in the converging light beam after the Hartmann screen. The positions of the images of the holes in the screen as recorded on the photographic plates or detector arrays give the transverse and longitudinal ray aberrations directly. It should be noted that if a single photographic plate or detector array is used, both the hole positions in the screen and the distance between the screen and plate must be known, while if two photographic plates or detector arrays are used, only the distance between the plates or detector arrays need be known.

One advantage of the Hartmann test for the testing of telescope mirrors is that effects of air turbulence will average out. Air turbulence will cause the spots to wander, but as long as the integration time is long compared to the period of the turbulence the major effect will be for the spots to become larger, and as long as the centroid of the spots can be accurately measured the turbulence will not introduce error in the measurement. The holes in the Hartmann screen should be made large enough so diffraction does not limit the measurement accuracy, but not so large that surface errors are averaged out.
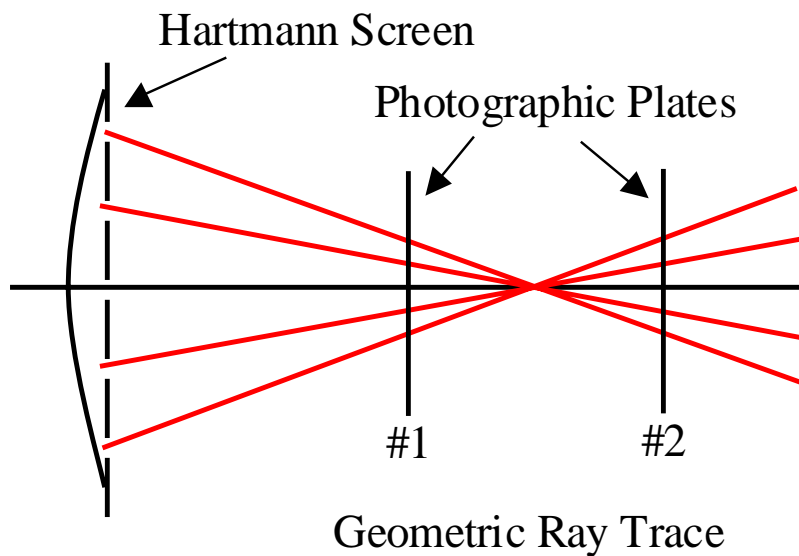
Fig. 1. Classical Hartmann test. Single photographic plate: must know (a) hole positions in screen, (b) distance between screen and plate. Multiple photographic plates: must know the distance between plates.

Figure 2 shows the results for testing a parabolic mirror at the center of curvature. Note that the detectors must be kept away from the caustic or much confusion can result. Once the transverse or longitudinal aberration is determined, the wavefront aberration can be determined.

Outside Position   **Inside Position**
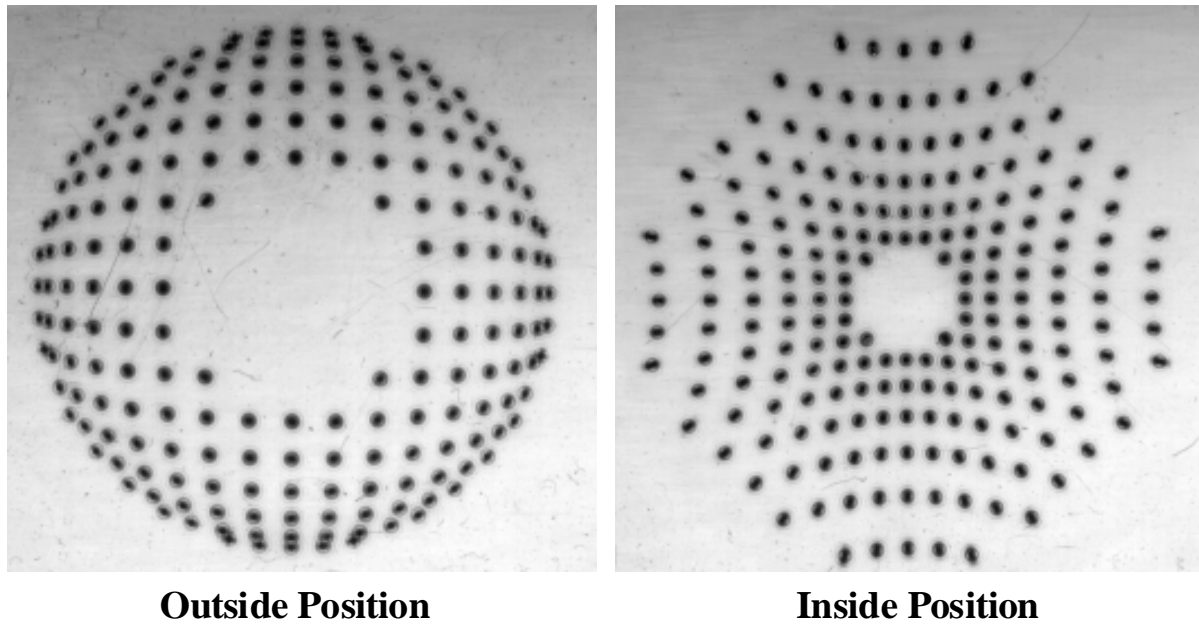
Fig. 2. Hartmann test of parabolic mirror near center of curvature.

Shack modified the Hartmann test by replacing the screen containing holes with a lenslet array. In typical use the beam from the telescope is collimated and reduced to a size of a few centimeters and impinges on a lenslet array that focuses the light onto a detector array as shown in Figure 3. The positions of the various focused points give the local slope of the wavefront. Figure 4 shows photos of a Shack-Hartmann lenslet array.
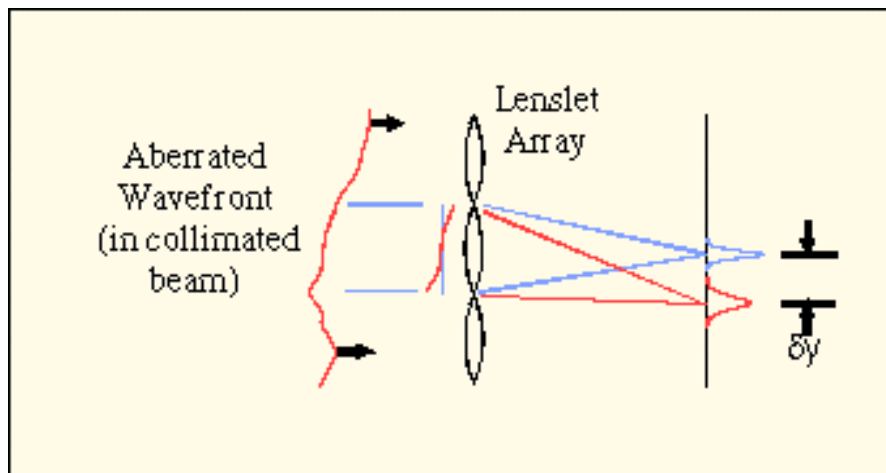
Fig. 3. Shack-Hartmann lenslet array measuring slope errors in an aberrated wavefront.

Fig. 4. Photos of a Shack-Hartmann lenslet array.

The Shack-Hartmann wavefront sensor is widely used in adaptive optics correction of atmospheric turbulence. Figure 5 shows a movie of the focused spots from the Shack-Hartmann test dancing around due to atmospheric turbulence.

Fig. 5. Movie made using Shack-Hartmann test to measure atmospheric turbulence.

WaveScope

WaveScope™ Wavefront Sensor System WFS-01
Table Top Optical Wavefront Sensor

Adaptive Optics Associates, Inc.

Adaptive Optics Systems (AOS) Group

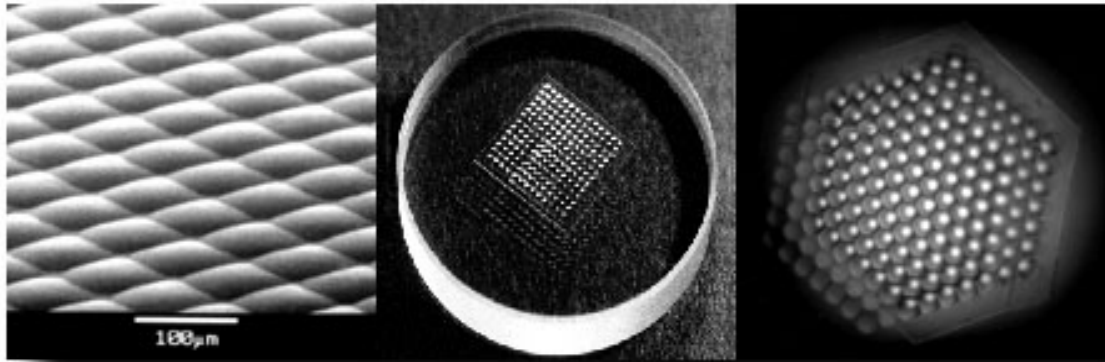54 CambridgePark Drive

Cambridge Massachusetts 02140-2308

aos@aoainc.com
www.aoainc.com/AOS/AOS.html

617 864-0201 Tel.
617 864-1348 Fax.

Wavefront Sensor System Model WFS-01 Features

• Replaces interferometers & beam profilers
• Insensitive to vibration
• Measures surfaces from millimeters to meters in diameter
• Works with monochromatic and white light
• Measures tilts up to 430 λ P-V @ 632.8nm
• Absolute accuracy < λ/20 @ 632.8nm
• Relative accuracy < λ/50 @ 632.8nm
• Powerful and easy to use analysis software
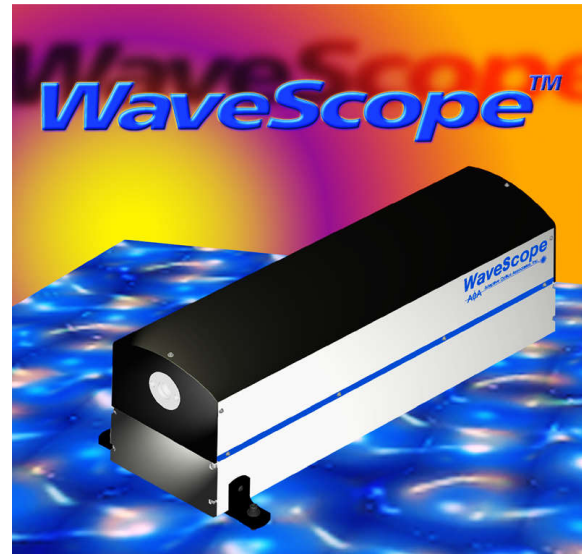
Applications

• External source measurements
• Laser beam profiler
• Lens testing
• Plane, spherical and aspheric mirror testing
• Precision mechanical component testing
• Atmospheric and fluid turbulence tests
• Quality and process control

Introducing WaveScope

WaveScope is a new generation of wavefront sensor. It incorporates innovations and knowledge gained by Adaptive Optics Associates (AOA) in its two decades of experience in the field of wavefront sensing. WaveScope uses a modified Shack-Hartmann technique to geometrically measure optical wavefronts.

WaveScope can perform the same measurements traditionally made by beam profilers and interferometers, but unlike interferometers, WaveScope does not require a coherent monochromatic source and is vibration insensitive. WaveScope calculates all common optical parameters using powerful software developed from AOA's WaveLab product. Since WaveScope needs no internal light source, it can directly measure the characteristics of your laser, light source or optical system.

WaveScope's dynamic range can be tailored to your requirements as WaveScope is unique in its ability to accommodate aberrations of many hundreds of waves P-V that are normally outside the range of interferometers and other wavefront sensors. This allows you to measure diverse optical systems, from high quality astronomical mirrors to consumer optics and precision metal or ceramic components. In quality and process control situations you can use signals derived from WaveScope to control manufacturing processes. WaveScope can also form the heart of an adaptive optics system. With the addition of simple fore-optics, the wavefront at any pupil within an optical train can be measured. Collimated and point source laser diode references are available as options.

AOA™ Adaptive Optics Associates, Inc.

Proven Performance

WaveScope has been developed from AOA wavefront sensors that have been used for several years by some of the world's most prestigious research institutions and optical companies, these include: US Air Force; French Atomic Energy Commission; Japanese Atomic Energy Research Institute; Japanese Central Research Laboratories; Contraves, Inc. and NASA. An AOA wavefront sensor helped fix the Hubble Space Telescope (HST) by verifying the performance of the corrective optics. Today NASA continues to use our system in its benchmark tests of optical systems for HST.
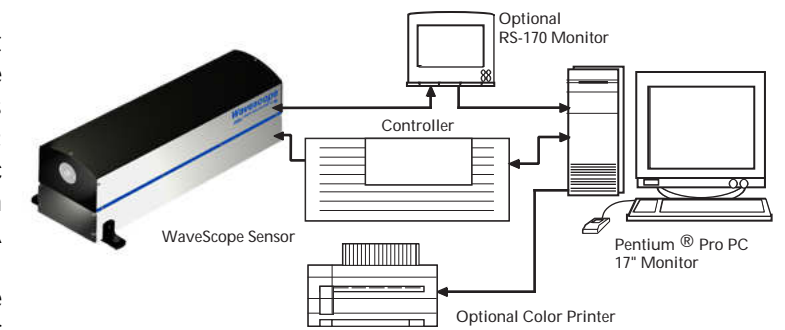
Customized Solutions and Decades of Experience

As a manufacturer of electro-optical instruments since 1978, AOA has the experience and technical staff to solve your wavefront sensing problems. If your requirements exceed those of our standard products, we will work with you to provide customized solutions: WaveScope can easily be tailored to your application. We can provide modified optics and CCD cameras that increase the dynamic range to thousands of waves P-V, increase the accuracy to better than one hundredth of a wave, or extend the operating wavelength from the near IR to the vacuum UV. For fast processes, high speed CCD cameras are available. Whatever your measurement needs WaveScope and AOA can provide a solution.

How it Works

WaveScope uses a modified Shack-Hartmann technique to measure the gradient of a wavefront. A two-dimensional Monolithic Lenslet Module (MLM) divides the incoming wavefront into an array of spatial samples called subapertures. Light from these subapertures is brought to a focus behind the array on a CCD camera. The lateral position of the focus spots depends on the local tilt of the wavefront. By measuring the positions of the spots, the gradients of the incoming wavefront can be calculated. In conventional Shack-Hartmann wavefront sensors when the local tilt is large enough to move the focus spot into the field of the next subaperture, an ambiguity arises as to the origin of the spot. This severely limits the dynamic range of the measurement. WaveScope resolves this ambiguity by moving the camera to trace the path of the spots during calibration. This is why WaveScope can measure aberrations of many hundreds of waves with fractional wave accuracy. Additionally, the ability to move the camera allows imaging of the entrance pupil at the lenslet array, which provides an invaluable aid in alignment.

WaveScope System Diagram

Optional RS-170 Monitor
Controller
WaveScope Sensor
Pentium ® Pro PC 17" Monitor
Optional Color Printer

WaveScope Ordering Information

WaveScope System

WFS-01	Visible light wavefront sensor with 3 MLMs, controller, CCD camera, computer and 17" color monitor.

WFS-01 Options:

WFS-01-VM	BW RS-170 video monitor
WFS-01-CM-P	Color printer
WFS-01-CM-JD	Jaz™ drive
WFS-01-CM-ZD	Zip™ drive

Reference Sources

RS-01	Collimated fiber coupled 635nm laser diode source
RS-02	Fiber optic point source 635nm laser diode source

Specifications
WFS-01 WaveScope System

Optical interface	1 cm Collimated beam
Input Pupil Shape	Circular, Square or Obscured
Wavefront Sampling	20 x 20, 32 x 32, and 72 x 72 MLM subapertures
Wavelength of Operation	400-900 nm
Maximum Measurable Tilt	430 λ P-V @ 632.8 nm
Absolute Accuracy (Gradient)	better than λ/20 @ 632.8 nm
Relative Accuracy (Repeatability)	better than λ/50 @ 632.8 nm
Operating Voltage	100-120 & 200-240VAC @50/60Hz
Measurements:	OPD, MTF, PSF, fringes, encircled energy, zernike, legendre, hermite, chebychev, monomials, seidel aberrations, wavefront gradients and beam profiles
Displays	Gradients, wire grids, color images and contours, plots and text
Peak power for modules	150 W approximate (with stage moving)
Computer power	720 W maximum
Monitor power	204 W
Optical module size/weight	54.2 cm x 15.3 cm x 17.2 cm, 17 kg
Electronics module size	14.6 cm x 34.6 cm x 24.7 cm, 12 kg